An ex vivo tumor fragment platform to dissect response to PD-1 blockade in cancer

Paula Voabil[1,2,9], Marjolein de Bruijn[1,9], Lisanne M. Roelofsen[1,9], Sanne H. Hendriks[1,7], Simone Brokamp[1], Marlous van den Braber[1,8], Annegien Broeks[3], Joyce Sanders[3], Petra Herzig[4], Alfred Zippelius[4], Christian U. Blank[1,5], Koen J. Hartemink[6], Kim Monkhorst[3], John B.A.G. Haanen[1,5], Ton N. Schumacher[1,2,10], and Daniela S. Thommen[1,10]*

[1]Division of Molecular Oncology & Immunology, Netherlands Cancer Institute, Amsterdam, The Netherlands
[2]Oncode Institute
[3]Department of Pathology, Netherlands Cancer Institute, Amsterdam, The Netherlands
[4]Department of Biomedicine, University Hospital Basel, Switzerland
[5]Department of Medical Oncology, Netherlands Cancer Institute, Amsterdam, The Netherlands
[6]Department of Surgery, Netherlands Cancer Institute, Amsterdam, The Netherlands
[7]Current address: Department of Immunohematology and Blood Transfusion, Leiden University Medical Center
[8]Current address: Department of Molecular Cell Biology and Immunology, Amsterdam UMC, VU University Medical Center, Amsterdam, The Netherlands
[9]These authors contributed equally
[10]These authors jointly supervised this work

*Correspondence should be addressed to d.thommen@nki.nl

Abstract

Inhibitors of the PD-1 – PD-L1 axis have been approved as therapy for numerous human cancers. In spite of the evidence for their widespread clinical activity, little is known on the immunological alterations that occur in human cancer tissue upon PD-1 blockade. We developed and employed a patient-derived tumor fragment (PDTF) platform to dissect the early immunological response of human tumor tissue to ex vivo PD-1 blockade. We observe that the capacity of immune cells to be reactivated ex vivo was predictive of clinical response, and perturbation analyses identify tumor-resident T cells as a key component of this immunological response. In addition, through combined analysis of baseline properties and immune response capacity we identify a novel subgroup of infiltrated tumors that lacks the capacity to respond to PD-1 blockade. Finally, the baseline presence of tertiary lymphoid structures and their components correlates with the capacity of cancers to undergo intratumoral immune cell reactivation.

Main text

Introduction

Immune checkpoint blockade targeting the PD-1/PD-L1 pathway has transformed cancer treatment in many tumor types. At present, PD-1 and/or PD-L1 blocking antibodies have been approved for 16 tumor types[1]. In addition, PD-1/PD-L1 blockade forms the backbone of 1,000s of ongoing clinical studies that evaluate combination immunotherapies in oncology[1]. In spite of the central role of PD-1/PD-L1 axis blockade in oncology, the immunological consequences of such blockade in human cancers remain incompletely understood. To provide three specific examples, recent data suggest (i) that PD-1 blockade may mainly target peripheral – rather than tumor-resident – T cells, as inferred from changes in the intratumoral TCR repertoire between pre- and on-treatment biopsies[2-4], (ii) that PD-1 blockade may to a substantial extent act via myeloid cells, as based on mouse models in which PD-1 is selectively absent on such cells[5], and (iii) that PD-1 and PD-L1 blockade may not necessarily be functionally equivalent, as based on evidence in preclinical models indicating that the latter can free up a pool of B7 molecules on APCs that may provide a costimulatory signal[6].

To assess how the immunological properties of human cancers are altered upon PD-1 blockade, a number of studies have compared pre- and on-treatment biopsies to evaluate, for instance, changes in the abundance of defined T cell populations, or changes in the intratumoral TCR repertoire[7,8]. While this approach is important to understand the longer-term consequences of immune checkpoint blockade, its value in deciphering the early effects of checkpoint blockade is limited. Notably, the observation of a 30% complete or major pathological response rate after a single cycle of anti-PD-1 in a recent neoadjuvant study in melanoma[9] underscores the importance of early changes in intratumoral immune activity. As a second limitation of current approaches, the use of serial biopsies does not allow one to directly compare the effects of different perturbations, complicating efforts to answer mechanistic questions.

Human ex vivo systems that maintain the tumor microenvironment (TME) and architecture as found in the patient, but that enable perturbation by immunotherapies, provide an opportunity to

study both the dynamics of treatment response and baseline properties of a tumor. In two recent studies, different technologies have been devised to investigate ex vivo responses to immune checkpoint blockade. In particular, a system using human air-liquid interface organoids consisting of both tumor and stroma components was shown to allow preservation of the intratumoral T cell repertoire and showed upregulation of interferon-γ (IFNγ), granzyme B and perforin expression upon PD-1 blockade[10]. Similarly, ex vivo treatment with anti-PD-1 and/or anti-CTLA-4 was shown to elicit cytokine secretion in patient-derived organotypic tumor spheroids[11]. However, a significant correlation between these immunological alterations and clinical response to immune checkpoint blockade was not established. The development of ex vivo models that can predict clinical response would be of particular value, as it would allow one to assess the effect of additional perturbations on the TME (see below), and thereby directly test the functional importance of specific cell types or cytokines in treatment response. Towards this goal, we developed and validated a patient-derived tumor fragment (PDTF) platform to assess the early immunological response of five different cancer types to ex vivo PD-1 blockade. We have subsequently used this platform to evaluate (i) whether early immunological response correlates with clinical response, (ii) whether there are baseline parameters that can predict immunological responsiveness, and (iii) whether distinct subtypes of immunologically non-responsive tumors can be identified. Our data demonstrate that the capacity of tumors to respond clinically to PD-1 blockade correlates with the capacity of already resident intratumoral immune cells to be reactivated by PD-1 pathway blockade. Furthermore, this immunological responsiveness is driven, at least in part, by pre-existing intratumoral T cells. In addition, we identify three subtypes of non-responsive tumors that differ in both the magnitude and location of the T cell infiltrate, but that share a lack of substantial tumor reactivity. Finally, the baseline presence of tertiary lymphoid structures and their components were shown to be predictive for the capacity of cancers to undergo immune cell reactivation upon PD-1 blockade.

Results

A human tumor fragment platform that preserves TME and architecture

To assess the early immunological responses of human cancers to PD-1 blockade, we developed an organotypic culture platform using patient-derived tumor fragments (Fig. 1a). In this platform, fresh tumor tissue from surgical resections is dissected into fragments of approximately 1mm^3, with the aim to allow sufficient nutrient and reagent access while preserving the cellular contexture and architecture of the tumor. Furthermore, the use of small-sized tumor fragments also allows the mixing of PDTFs from different tumor areas, thereby reducing the confounding effects of tumor heterogeneity (Extended Data Fig. 1a). In order to prevent immune cell efflux, PDTFs were embedded in artificial extracellular matrix (Extended Data Fig. 1b,c). To assess stability of the tissue during culture, T cell, non-T cell, and non-immune cell compartments, as well as cytokine and chemokine secretion, were analyzed at different timepoints. Stable levels of cellular and soluble factors were observed up to 48 hours of culture (n=4), indicating that this system allows the analysis of early effects of ex vivo treatment (Extended Data Fig. 1d). By comparing PDTF cultures with and without matrix, we confirmed that embedding in matrix did not limit T cell functionality or induce unspecific immune activation (Supplementary Fig. 1a-d). Penetration of exogenously added antibodies into PDTFs was validated by both flow cytometry and immunofluorescence staining (Extended Data Fig. 1f), and parallel cultures of PDTFs from six tumors showed comparable patterns of steady state secretion of soluble factors for all matched samples, providing a measure of the reproducibility of the data obtained (Extended Data Fig. 1e). Jointly, these and additional data (Supplementary Fig. 1e-h) validate PDTFs as a platform to assess the functional importance of certain cell types or cytokines upon ex vivo immunotherapeutic perturbation.

Immunological response of human cancers to PD-1 blockade

To evaluate the immunological response to PD-1 blockade in distinct human cancers (relevant controls shown in Extended Data Fig. 2a-c), we profiled the effect of PD-1 blockade on 37 tumors from

five different cancer types (melanoma, non-small cell lung cancer (NSCLC), breast cancer, ovarian cancer and renal cell carcinoma) (Extended Data Fig. 2d), using 13 cytokines, 13 chemokines, and 4 T cell activation markers as readouts. For each parameter, normalized delta values between the anti-PD-1 treated and untreated condition were determined and used for unsupervised hierarchical clustering. This analysis revealed two broad groups of tumors: a larger group that showed only minor treatment-induced changes in all of the assessed parameters (24/37 tumors, hereafter referred to as PDTF non-responders, PDTF-NR), and a smaller group of tumors (13/37) that displayed a clear increase in immune activity upon ex vivo PD-1 blockade (PDTF responders, PDTF-R) (Fig. 1b). The immunological responder group was dominated by melanoma and NSCLC samples, but also contained two ovarian cancers. Principal component analysis resulted in a similar division between PDTF-NR and PDTF-R samples and indicated a further subdivision of PDTF-R tumors based on distinct response patterns (Fig. 1c). While response patterns were reproducible in independent PDTF cultures from the same tumor (Extended data Fig. 3a), analysis of individual tumor fragments, rather than pooled tumor fragments, demonstrated intratumoral heterogeneity in response capacity (Extended Data Fig. 3b-c). Modeling of these data emphasized the need to average PDTF responses over a series of approximately eight tumor fragments (Extended Data Fig. 3d), as done in all standard PDTF cultures.

AUC analysis of individual parameters revealed that the separation of PDTF-R and PDTF-NR tumors was mostly driven by a subset of parameters, including CXCL1, IFNγ and CXCL10 (see also below), and this information was used to establish a PDTF response score based on the most discriminative parameters (Extended data Fig. 4a-c). To understand whether these ex vivo immunological responses of resected lesions would correlate with clinical response, we focused on the 12 patients who subsequently received PD-1 blocking therapy. Even though immunological response was in some cases assessed on lesions that were resected during an earlier disease stage, ex vivo PDTF response and clinical response correlated in 12/12 cases (p=0.0013, Fig. 1d, clinical response reflects best radiological response). To further understand the relationship between ex vivo PDTF response and clinical response, an additional cohort of 26 patients with matched clinical response

data, including melanoma and NSCLC lesions obtained from 12 patients that did not respond to clinical PD-1 blockade, was assessed. For the 3 patients experiencing a mixed response, an immunological response was observed in 2/3 cases. For the 23 patients achieving either a partial or complete response (n=5), or showing stable or progressive disease (n=18), clinical outcomes were in all cases in full concordance with the immunological response ($p<0.0001$) (Fig. 1d). To understand whether different tumor lesions of a patient show heterogeneity in their immunological response, we assessed ex vivo anti-PD-1 responses in PDTFs from 11 patients for whom multiple lesions could be collected. Of note, in 8/11 (73%) patients we observed concordant immunological responses (Extended data Fig. 4d). The majority of samples in our cohort was derived from primary tumor lesions (Extended Data Fig. 2d, Supplementary Table 1), and the PDTF-R group showed a slight enrichment for lymph node metastases (4/13 compared to 4/24 PDTF-NR). To determine whether the immunological responses observed were mainly driven by lymph node metastases, anti-PD-1 responses in PDTFs from 27 lymph node metastases and 18 lesions of primary tumors or distant metastases were compared, showing similar ranges of the response score between the two groups (Extended data Fig. 4e). Jointly, the above data indicate that clinical response to anti-PD-1 therapy correlates with the capacity of tumor-resident immune cells to be (re-)activated by PD-1/PD-L1 pathway blockade.

Tumor-resident T cells drive the response to PD-1 blockade

Prior work has provided evidence for a role of T cells in the activity of PD-1 blocking antibodies[12], and the high-level expression of PD-1 on human tumor-reactive T cells is in line with this model[13-15]. However, it is presently unclear, whether tumor-resident T cells can be reactivated by PD-1 blockade, or whether treatment mainly mobilizes peripheral T cells as recently suggested[2,3]. Analysis of T cell activation markers, as well as the T cell effector cytokines IL2, TNFα and IFNγ, revealed detectable increases upon ex vivo PD-1 blockade in PDTF-R tumors (Fig. 2a, Extended Data Fig. 5a). Importantly, tumor-resident T cells in PDTF-NR tumors did not respond to PD-1 blockade, but could be activated by anti-CD3 antibodies (Extended Data Fig. 5b,c), indicating that these T cells can respond

to TCR triggering, and that the PD-1 – PD-L1 axis is not a critical signaling pathway that limits the physiological activity of this T cell pool. PD-1 blockade further induced the release of multiple cytotoxicity markers including perforin, granzymes A and B, and granulysin in PDTF-R tumors, suggestive of reactivation of an intratumoral cytotoxic T or NK cell response (Fig. 2b,c). Importantly, not only parameters that directly reflect T cell activation, such as CD137 expression and IL2 and IFNγ production, but also IFNγ target molecules, such as the CXCL9 and CXCL10 chemokines, were increased by PD-1 blockade. In addition, induction of a series of other chemokines, including CXCL1, CXCL5, CCL17 and CCL20, was significantly associated with response (Fig. 2d,e, Extended Data Fig. 6).

Recent work from Strauss et al. has provided clear evidence that PD-1 blockade may not only act on T cells, but that PD-1 expression on myeloid cells may contribute substantially to the activity of PD-1 blocking therapies in mouse models[5]. To understand to what extent the observed immune reactivation in human cancers could be modulated by either preventing T cell receptor signaling or downstream IFNγ receptor signaling, we pretreated PDTFs from eight responding tumors with either a lymphocyte-specific protein tyrosine kinase inhibitor (LCKi), or with an IFNγR1 blocking antibody (aIFNγR1, optimal concentrations identified by titration experiments using anti-CD3/anti-CD28 stimulated PBMCs, Extended Data Fig. 7a-c). Preincubation of PDTFs with aIFNγR1 antibody abolished part of the anti-PD-1 response, with the most profound effects on IFNγ-induced molecules such as CXCL9, CXCL10 and CXCL11, on $CD4^+$ T cell cytokines such as IL21, as well as on the chemokines CCL3 and CCL5 (Fig. 2f, Extended Data Fig. 7d,e). Notably, inclusion of LCKi prevented anti-PD-1-induced immune reactivation for most parameters (Fig. 2f, Extended Data Fig. 7d,e). In addition, Lck inhibition in PDTF-R tumors not only abolished immune activity upon PD-1 blockade, but reduced immune activity below the levels present during steady-state (Fig. 2g,h, Extended Data Fig. 7d,e). Jointly, these data provide evidence that immune reactivation following PD-1 blockade is to a large part dependent on tumor-resident T cells. In addition, the data imply that the T cell pool in these tumors is generally not fully inert prior to PD-1 blockade, but is characterized by a low-level steady-state anti-tumor response.

Subtypes of immunologically non-responsive tumors

Having established that pre-existing immune cells can be reactivated in only part of human tumors, we wished to explore whether baseline properties of tumors can predict capacity for immune reactivation by PD-1 blockade. Prior studies have indicated that the level and type of immune infiltrate of human tumors are associated with clinical response to immunotherapy[16-19]. Jointly, these studies have led to the definition of three major tumor subgroups: immune desert tumors in which immune cells are largely absent, excluded tumors in which the T cell compartment is primarily peritumoral, and infiltrated tumors in which the T cell infiltrate is observed amongst tumor cell nests. To investigate whether the differences in the observed immunological response of human cancers to PD-1 blockade could be explained by distinct immune contextures, we first quantified immune cell fractions by flow cytometry (Extended Data Fig. 8a). This revealed a subgroup of tumors (10/37, 27%) that lacked a substantial immune compartment (<10% immune cells). In line with expectations, 0/10 of these tumors had been identified as PDTF responders (Fig. 3a,b). Amongst the remaining 27 tumors, an immune cell compartment of comparable magnitude was observed for non-responding and responding tumors, with an enrichment in B cells in the latter (Fig. 3a, Extended Data Fig. 8b, see below). To understand whether the presence of $CD8^+$ T cells either inside or outside of tumor cell nests could be used to further identify tumors that respond to PD-1 blockade, we performed digital image analysis of $CD8^+$ T cells in tumor and stromal areas (Fig. 3c, Extended Data Fig. 8c). While $CD8^+$ T cells were generally more abundant in stromal areas and total numbers differed across cancer types (Extended Data Fig. 8d), distinct spatial patterns could be identified. Importantly, within the immune cell rich tumors (n=26, no IHC data available for BR015), this analysis identified seven tumors with an excluded $CD8^+$ T cell pool, where $CD8^+$ cells were present in stromal areas, but not or at very low numbers within tumor regions. Notably, 6/7 of these tumors did not show immune reactivation upon PD-1 blockade (Fig. 3c). Thus, of the tumors that were characterized as either immune deserts or as $CD8^+$ T cell excluded, only 1/17 (5.9%) showed immune cell reactivation upon ex vivo PD-1 blockade,

potentially explaining the low clinical response rates previously observed in tumors with such microenvironments[7,16]. In contrast, immune cell reactivation upon PD-1 blockade was observed in 12/19 $CD8^+$ infiltrated tumors.

To understand the basis for differences in immunological response capacity within the final subgroup of $CD8^+$ infiltrated tumors, we classified the PDTF cohort into four tumor microenvironment (TME) types – immune deserts, $CD8^+$ excluded, $CD8^+$ infiltrated PDTF-NR and $CD8^+$ infiltrated PDTF-R tumors. Subsequently, we compared these groups with respect to four different properties: (1) The presence of a baseline inflammatory signature, (2) The differentiation states of tumor-resident myeloid cells and T cells, (3) The presence of a tumor-reactive T cell compartment, and (4) The evidence for the formation of tertiary lymphoid structures (TLS).

Baseline chemokine production and immune cell states across TME types

Analysis of cytokine and chemokine production after 48 hrs of PDTF culture without treatment revealed heightened baseline activity in PDTF-R tumors, not only when compared to immune desert tumors and $CD8^+$ excluded tumors, but also when compared to $CD8^+$ infiltrated PDTF-NR tumors (Fig. 3d,e, Extended data Fig. 9, Supplementary Fig. 2). Parameters for which baseline production predicted capacity for immune reactivation by PD-1 blockade included molecules such as CXCL9 and 10 that may reflect low level baseline T cell activity, but also the chemokine CXCL13 that is associated with the formation of TLS (Fig. 3f,g, Extended Data Fig. 9). In addition, high IL8 secretion showed a trend towards association with anti-PD-1 non-responsiveness, in particular in infiltrated PDTF-NR (Fig. 3f, Extended Data Fig. 9, Supplementary Fig. 2), an observation that deserves follow-up in view of prior data that have documented increased serum IL8 levels in non-responders to immune checkpoint blockade[20-22].

To understand whether the TME groups differed with regard to the cell states of infiltrating myeloid and T cell populations, we assessed both cell populations by flow cytometry. The immune infiltrate in PDTF-R tumors generally contained fewer myeloid cells, particularly compared to

infiltrated PDTF-NR and immune desert tumors (Supplementary Fig. 3a). An exploratory analysis of the composition of the myeloid cell pool revealed substantial variation across tumors (Supplementary Fig. 3b-e). While different frequencies of specific myeloid subsets were observed across TME subgroups, no subsets that were unique or predominant in a microenvironment were observed (Supplementary Fig. 3f,g). As persistent antigen stimulation and immunosuppressive stimuli in the TME can induce a progressive dysfunctional state in T cells that is accompanied by overexpression of multiple immune checkpoints[23-25], we next examined whether the expression of inhibitory receptors may predict capacity for immune reactivation upon PD-1 blockade. To this end, we assessed expression of PD-1, CTLA-4, Tim-3, Lag-3, and TIGIT on $CD8^+$ T cells (Fig. 4a). No significant difference in the fraction of inhibitory receptor-positive cells was observed between PDTF-Rs and infiltrated or excluded PDTF-NRs, except for a trend towards more frequent TIGIT expression in PDTF-R tumors. Surprisingly, immune deserts stood out by the frequent very high expression of several immune checkpoints on the few T cells present (Fig. 4b). In addition, immune deserts harbored the largest fraction of $CD8^+$ T cells that showed co-expression of multiple immune checkpoints (Fig. 4c, Extended Data Fig. 10a).

Recent data in murine cancer models and human melanoma[26-29] indicate that the dysfunctional T cell pool can be further subdivided into a progenitor or pre-dysfunctional population that is characterized by the expression of the transcription factor TCF-1, and a more differentiated, dysfunctional population that is TCF-1 negative but expresses CD39. Importantly, the $TCF\text{-}1^+$ pre-dysfunctional subset has been shown to be essential for durable responses to immunotherapy in mouse models[26-28] as well as in patients undergoing adoptive T cell therapy[30]. To understand whether a difference in pre-dysfunctional and dysfunctional subsets exists between PDTF-R and PDTF-NR tumors, we quantified $TCF\text{-}1^+$ and $CD39^+$ cells within the $PD\text{-}1^+CD8^+$ T cell pool. In line with previous data, TCF-1 was expressed in a subset of T cells that showed an intermediate PD-1 expression level and was mostly negative for CD39. In contrast, the $CD39^+$ subset was largely $TCF\text{-}1^-$ and expressed PD-1 at a very high level (Fig. 4d). The $TCF\text{-}1^+$ pre-dysfunctional population could be identified in excluded

and infiltrated TME types without a difference between responding and non-responding tumors (Fig. 4e, Extended Data Fig. 10b). However, the balance between the pre-dysfunctional and dysfunctional subset was strongly skewed towards the latter in immune deserts, indicating that the pre-dysfunctional pool may be lacking in part of these tumors (Fig. 4e,f, Extended Data Fig. 10b,c).

Tumor reactivity varies in responding and non-responding tumors

The co-expression of CD39 and CD103 has been shown to identify tumor-reactive T cells in solid tumors[31]. Similarly, $CD8^+$ T cells with a PD-1 expression level that exceeds that found on peripheral blood T cells, so-called PD-1^T TILs, have been shown to display an enhanced capacity for tumor recognition in NSCLC[15]. To understand whether the prevalence of these T cell subsets may correlate with the capacity for immunological response to PD-1 blockade, we quantified $CD39^+CD103^+$ and PD-1^T $CD8^+$ T cell subsets in the different TME subgroups (Fig. 5a,b, Extended data Fig. 10c-e). Notably, while expression of the tissue residency marker CD103 alone, which has been shown to be associated with response to PD-1 blockade in prior studies[32-34], was comparable between TME subgroups (Extended Data Fig. 10d), the fraction of $CD39^+CD103^+$ double positive cells was highest within $CD8^+$ T cells in PDTF-R and immune desert tumors, and a similar observation was made for PD-1^T TILs (Fig. 5c, for absolute numbers, see below). To directly test for the presence of a tumor-specific T cell pool, $CD3^+$ TILs from five PDTF-R and six PDTF-NR tumors were sorted and expanded, and tumor reactivity was determined by co-culture with autologous tumor digests (Fig. 5d, controls in Extended Data Fig. 10f). Notably, in all TIL obtained from PDTF-R tumors, tumor reactivity amongst $CD8^+$ TILs was detected and tumor reactivity amongst $CD4^+$ TILs was detected in 4/5 cases. In PDTF-NR tumors, tumor reactivity amongst $CD8^+$ TILs and amongst $CD4^+$ TILs were both detected for only 1/6 tumors (Fig. 5d, Extended Data Fig. 10g).

TLS and their components are predictive for response to PD-1 blockade

Jointly, the above analyses indicate that the capacity of a tumor to respond to PD-1 blockade may be related both to the magnitude of the T cell infiltrate as well as to the frequency of T cells with phenotypic characteristics of tumor-reactive T cells, such as high PD-1 expression or CD39/CD103 co-expression. Based on these two separate observations, we subsequently explored the predictive value of the absolute number of PD-1^T TILs, thereby combining the quantity and quality of tumor-resident T cells in a single metric. Both PD-1^T $CD8^+$ T cells, PD-1^T $CD4^+$ T cells, as well as total PD-1^T $CD45^+$ lymphocytes were increased in responding tumors (Fig. 6a-c), with PD-1^T lymphocytes showing the best discrimination between PDTF-R and all other TME types independent of cancer type. Prior work has established two characteristics of PD-1^T TILs that link these cells to tertiary lymphoid structures (TLS): first, PD-1^T TILs constitutively produce CXCL13, which is a crucial chemoattractant for the formation of TLS[35]. Second, in human NSCLC, PD-1^T TILs have been shown to be predominantly localized within TLS[15]. We therefore subsequently assessed whether the presence of TLS or their components was associated with the capacity of a tumor to respond to PD-1 blockade. Quantification of TLS in PDTF-R and PDTF-NR tumors by CD20 and CD3 staining (Fig. 6d) revealed that both TLS number and size (defined as average TLS area) were significantly higher in PDTF-R tumors, especially when compared to infiltrated PDTF-NR tumors (Fig. 6e). Notably, B cells, which are a major component of TLS, were also significantly enriched in PDTF-R tumors (Fig. 6f). To compare the potential of all parameters assessed in this study to predict the capacity of the intratumoral immune compartment to respond to PD-1 blockade, we analyzed the AUC [ROC] for PD-1^T lymphocytes, CXCL13, B cells, TLS number and TLS area. All five of these parameters strongly associated with anti-PD-1 response capacity, reaching an AUC ≥0.84 (Fig. 6g), indicating a high potential to identify those human tumors in which intratumoral immune activity is held back by the PD-1 checkpoint.

Discussion

Here we provide a comprehensive analysis of the early intratumoral immune response to PD-1 blockade in five different human cancer types, as well as the tumor properties that predict this

response. Using a patient-derived tumor fragment system as the approach to perturb tumor microenvironments, we observe that such immunological responses can already be detected within 24-48 hours after anti-PD-1 treatment in distinct cancer types. Importantly, these data provide the first evidence that capacity for intratumoral immune reactivation correlates closely with clinical response.

Seemingly contradictory data has been generated with respect to the question whether PD-1 blockade mainly reinvigorates tumor-resident T cells[27,36], or acts via recruitment of new T cell clones to the tumor site, a phenomenon referred to as 'clonal replacement'[2,4]. While observations made in lymph node samples may be more difficult to interpret, the current data obtained in non-lymph node lesions (9/13 PDTF-R) provide strong evidence that PD-1 blockade can reactivate pre-existing intratumoral T cells in human cancer lesions. Of note, as such reactivation is accompanied by increased production of T cell chemoattractants such as CXCL9, CXCL10, CCL5 and CXCL13, the current data are consistent with a model in which this reactivation may be a driver of the clonal replacement that has been observed in patients at later time points. Further work is required to understand whether PD-1 blockade can induce a durable reactivation of the already tumor-resident T cells, or whether their capacity for reinvigoration may be limited in time, e.g. due to fixed epigenetic changes[37,38]. We also note that the effects of Lck inhibition provide evidence for a smoldering T cell response in tumors that can be increased by PD-1 blockade. Thus, PD-1 blockade does not appear to reactivate a dormant, but rather boost an ongoing T cell response.

Notably, while in some tumors non-response could be explained by either lack of immune cells or exclusion of $CD8^+$ T cells, consistent with clinical data[7,16,17], we here identify a third subgroup of immunologically non-responsive tumors that is characterized by a brisk intratumoral $CD8^+$ T cell infiltrate, but that largely lacks the secretion of proinflammatory cytokines and chemokines. Importantly, as based both on T cell phenotype and on direct testing of tumor reactivity, the capacity of the tumor-resident T cell pool to recognize tumor antigens appears to distinguish PD-1 responsive tumors from the three non-responsive tumor microenvironments we identify.

The phenotype of the T cells detected in immune desert tumors analyzed here forms an outlier, with the few T cells present being strongly skewed towards a late dysfunctional state, and with a depletion of the pre-dysfunctional T cells that are detected in responding tumors. While further data are required, it may be speculated that these T cells represent the remainder of a 'failed immune response' in tumors that were once inflamed but have subsequently turned cold. The use of technologies that allow profiling of tumor reactivity of the intratumoral TCR repertoire in an unbiased manner[39], should be helpful to settle this issue. In such analyses, it will be useful to focus not only on the immune deserts amongst the melanoma, renal and lung cancers that are mostly represented here, but also include other 'cold' tumor types such as, for instance, pancreatic cancer.

The strong correlation between ex vivo response and clinical response raises the question whether the PDTF platform could allow prospective assessment of individual patient responses to PD-1 blockade. This may either entail the direct clinical application of the platform itself in addition to established biomarkers, such as PD-L1[16] or tumor mutational burden[40], or by deriving biomarker (patterns) that can be measured using other less complex assay systems. In our view, the latter approach, with the PDTF platform primarily being exploited to dissect reactivity patterns and link these to tumor baseline properties would be most attractive.

Finally, paralleling the recent data that link the presence of tertiary lymphoid structures (TLS) with clinical response to anti-PD-1 therapy[41-43], the current data reveal a link between the presence of TLS and capacity of intratumoral T cells to be reactivated by PD-1 blockade. Importantly, in addition to B cells, also the dysfunctional PD-1^{T} TILs that have been shown to be enriched in tumor reactivity predominantly localize in TLS[15], suggesting that the presence of these immune cell aggregates may be reflective of a structured ongoing anti-tumor immune response. In future work, combination of the PDTF platform described here with spatial profiling technologies[44-46] should allow one to determine whether TLS should solely be seen as hallmarks of inflamed tumors, or whether these sites form the actual hotbeds for immune reactivation upon PD-1 blockade in human cancer tissue.

Online Methods

Patient characteristics and tumor sample processing

Tumor samples were collected from individuals with melanoma, non-small cell lung cancer, breast cancer, ovarian cancer, or renal cell carcinoma undergoing surgical treatment between April 2017 and January 2020 at the Netherlands Cancer Institute (NKI-AVL), The Netherlands. Detailed patient characteristics are provided in Supplementary Table 1, 2 and 3. The study was approved by the institutional review board of the NKI-AVL and performed in compliance with all relevant ethical regulations. All patients consented to research usage of material not required for diagnostic use either by opt-out procedure or via prior informed consent (after May 23, 2018).

Solid tumor lesions were macroscopically selected by a pathologist from the resected tumor material and part of the tumor was collected in ice-cold collection medium (RPMI 1640 medium (Thermo Fisher) supplemented with 2.5% fetal bovine serum (FBS, Sigma), 1% Penicillin-Streptomycin (Roche)) for subsequent PDTF cultures. A second part of the tumor was embedded in paraffin for histological analysis and for analysis of tumor cell content within the collected lesion. Tissue materials collected for subsequent PDTF cultures were immediately processed by manual cutting into small tumor fragments (PDTFs) of 1-2 mm^3 size on ice. After processing, a number of single PDTFs from different regions within a tumor were mixed to ensure uniform representation of the tumor lesion (Extended Data Fig. 1a), and were frozen in cryovials containing 1 ml FBS with 10% DMSO (Sigma) with 8-15 PDTFs per vial. All PDTFs were cryopreserved in liquid nitrogen until further usage.

Patient-derived tumor fragment (PDTF) cultures

To prevent lymphocyte efflux, individual PDTFs were embedded in artificial extracellular matrix, prepared as follows: first, sodium bicarbonate (Sigma, 1.1% final concentration), collagen I (Corning, 1 mg/mL final concentration) and tumor medium (DMEM (Thermo Fisher) supplemented with 1mM sodium pyruvate (Sigma), 1× MEM non-essential AA (Sigma), 2 mM L-glutamine (Thermo Fisher), 10% FBS (Sigma) and 1% Penicillin-Streptomycin (Roche)) were slowly mixed. All components

were kept ice-cold to avoid premature solidification of the collagen. Next, ice-cold matrigel (Matrix High Concentration, Phenol Red-Free, BD Biosciences, 4 mg/mL final concentration) was very slowly added to the mix. To prepare tumor matrix that only contains collagen, the last step was omitted. For matrices with distinct glucose concentration, the standard DMEM medium (4,500 mg/L D-glucose) was replaced with either low glucose DMEM (1,000 mg/L D-glucose, Thermo Fisher) or RPMI 1640 (2,000mg/L D-glucose). To assess the effect of the type or concentration of serum, either 2% or 20% FBS (Sigma) or 10% human serum (Sigma) were used instead of 10% FBS. Each well of a pre-cooled 96-well plate was coated with 40 μL of matrix to serve as a bottom layer and matrix was solidified by exposure to 37°C for 20-30 min.

Vials with cryo-preserved PDTFs were thawed in a water bath at 37˚C until only a small drop of ice remained. PDTFs were then transferred into a 50 mL tube and slowly thawed by dropwise addition of 10 ml pre-warmed tumor medium. Next, PDTFs were extensively washed in tumor medium by flushing them multiple times on a cell strainer in a 6-well plate. One PDTF per well was placed on top of the pre-solidified matrix, after which a second layer of 40 μL matrix was added. Plates were then placed in a 37 °C incubator for 20-30 min. After solidification, 120 μL of tumor medium was added on top of the matrix. Where indicated, tumor medium was supplemented with either anti-PD-1 antibody (nivolumab, Bristol-Myers Squibb) at 10 μg/mL final concentration, or anti-CD3 (OKT3, Biolegend) at 5 μg/mL final concentration either alone or in combination with anti-CD28 (CD28.2, Biolegend) at 2 μg/mL final concentration. Control cultures were carried out in the presence of control human anti-β-Gal-hIgG4 (S228P, InvivoGen) at 10 μg/mL. 8 to 10 PDTFs were used per condition. Unless indicated otherwise, PDTF cultures were kept at 37 °C for 48 hrs before readout.

Flow cytometric analysis of PDTFs

PDTFs were analyzed by flow cytometry to assess T cell activation after culture, and to determine immune cell composition and T cell state at baseline using the following antibodies: T cell activation analysis: anti-CD45 PerCP Cy5.5 (2D1, 1:100), -CD3 APC-eFluor780 (SK7, 1:50), and -ICOS

FITC (ISA-3, 1:25), all from Invitrogen; anti-CD3 FITC (SK7, 1:50), -CD8 BV605 (RPA-T8, 1:100), -CD4 BV421 (SK3, 1:100), -OX40 APC (BerACT35, 1:20), and -CD25 AF700 (BC96, 1:20), all from Biolegend; anti-PD-1 PE-Cy7 (EH12.1, 1:20), -CD137 PE (4B4-1, 1:20), and -CD137 BUV395 (4B4-1, 1:50), all from BD Biosciences; anti-IFNγR1 PE (92101, 1:25), from R&D systems. Immune composition and T cell state analysis: anti-CD45 PerCP Cy5.5 (2D1, 1:100), -CTLA-4 FITC (14D3, 1:50), -TIGIT PE (MBSA43, 1:20), and -LAG3 :APC (3DS223H, 1:20), all from Invitrogen; anti-CD8 BUV563 (RPA-T8, 1:50), -CD3 BV711 (UCHT1, 1:50), -PD-1 PE-Cy7 (EH12.1, 1:20), and -CD103 BV421 (Ber-ACT8, 1:20), all from BD Biosciences; anti-CD3 FITC (SK7, 1:50), -CD4 BV421 (SK3, 1:100), -CD19 BV605 (SJ25C1, 1:50), -FoxP3 AF647 (259D, 1:50), -CD11c PE (Bu15, 1:50), -CD16 Alexa 700 (3G8, 1:50), -TIM-3 BV421 (F38-2E2, 1:20), -CD39 FITC (A1, 1:20), and - TCF1 PE (7F11A10, 1:20), all from Biolegend. Myeloid cell, fibroblast and endothelial cell analysis: anti-CD45 PerCP-Cy5.5 (2D1, 1:100), from Invitrogen; -lineage cocktail CD3/CD19/CD20/CD56 APC (UCHT1, HIB19, 2H7, 5.1H11, 1:50), -CD11b BV605 (ICRF44, 1:50), -CD68 FITC (Y1/82A, 1:50), -CD206 PE-Cy7 (15-2, 1:20), -CD14 AF700 (M5E2, 1:200), -CD123 BV421 (6H6, 1:100), -PD-L1 (29E.2A3, 1:100), all from Biolegend; anti-CD11c PE-CF594 (3.9, 1:200), -HLA-DR BUV395 (L243af, 1:100), -CD31 BV480 (WM-59, 1:100), -CD86 BUV563 (FUN-1, 1:50), all from BD Biosciences; anti-FAPα PE (427819, 1:20), from R&D systems.

For analysis of PD-1 blockade effects, PDTFs were manually retrieved from the matrix after 48 hrs of culture, pooled for each experimental condition and processed into single-cell suspensions by enzymatic digestion in digestion mix (RPMI 1640 medium (Thermo Fisher) supplemented with 1% Penicillin-Streptomycin (Roche), 12.6 µg/mL Pulmozyme (Roche) and 1 mg/mL Collagenase type IV (Sigma)) for 1 h at 37°C and under slow rotation. Samples were then washed in PBS (Sigma), filtered over a 150 µM filter mesh, resuspended in 50 µL PBS, and incubated with Fc receptor blocking agent (eBioscience) and with either live/dead IR Dye (Thermo Fisher) or Zombie UV (Biolegend) for 20 min at 4°C. Cells were washed, resuspended in 50 µl of staining buffer (PBS (Sigma), 0.5% bovine serum albumin (Sigma), 0.1% NaN_3 (Invitrogen)) containing the above-described antibodies, and incubated

for 20 min at 4°C. After washing twice, cells were taken up in 200 µl IC Fixation Buffer (eBioscience) and incubated for 20 min. Subsequently, samples were washed twice before data acquisition.

For analysis of immune infiltrates and T cell states, PDTFs were thawed and immediately digested as described above. Samples were resuspended in 50 µL PBS and incubated with Fc receptor blocking agent (eBioscience) and with either live/dead IR Dye (Thermo Fisher) or Zombie UV (Biolegend) for 20 min at 4°C. Cells were then washed, resuspended in 50 µL of staining buffer containing the above-described antibodies, and incubated for 20 min at 4°C. For intracellular staining, cells were washed twice, fixed and permeabilized using Fix/Perm solution (eBioscience) for 30 min at room temperature. After washing twice, cells were resuspended in 1x Permeabilization Buffer (eBioscience) containing antibodies for 40 min at room temperature. Subsequently, samples were washed twice before data acquisition.

Data acquisition was carried out on a BD LSR II SORP, a Fortessa SORP, or a Symphony A5 SORP cell analyzer (all from BD Biosciences). Data was collected using the BD FACS Diva Software version 8.0.1 (LSR II SORP), version 8.0.2 (Fortessa SORP), and version 8.5 (A5 SORP), and further analyzed with FlowJo v10.6.1 (Tree Star Inc.) and GraphPad Prism v8.0e (GraphPad Software Inc.). Analysis of co-expression of inhibitory receptors was performed using SPICE[47]. Clustering analyses were performed using the FlowJo plugins UMAP[48] and X-Shift[49]. An example of the gating strategy is shown in Supplementary Figure 4.

Immunohistochemistry and digital image analysis

Immunohistochemistry of sectioned tumor samples was performed on a BenchMark Ultra autostainer Instrument (Roche). In brief, serial 3 µm sections were cut from formalin-fixed paraffin embedded tumor samples. Sections were heated at 75°C for 28 min and deparaffinised in the Instrument with EZ prep solution (Ventana Medical Systems). Heat-induced epitope retrieval was carried out using Cell Conditioning 1 (CC1, Ventana Medical Systems) for 32 min at 95°C (CD4, CD8, CD3 and CD20), or for 48 min at 95 °C (PD-1). Sections were then stained with monoclonal antibodies

against CD4 (SP35, 1:25, Cell Marque), CD8 (C8/144B, 1:200, DAKO/Agilent), CD20 (L26, 1:800, DAKO/Agilent), CD3 (SP7, 1:100, Spring/ITK) for 32 in at 37˚C and PD-1 (NAT105, Ready-to-Use, Roche) for 16 min at room temperature. Antibodies were detected using 3,3'-diaminobenzidine (DAB, OptiView Detection Kit, Ventana Medical Systems). Slides were counterstained with Hematoxylin and Bluing Reagent (Ventana Medical Systems).

Slides were scanned at x20 magnification using an Aperio slide AT2 scanner (Leica Biosystems) and data were uploaded on Slide Score (www.slidescore.com). Tumor lesions were digitally annotated using the HALO™ image analysis software version 2.3 (Indica Labs). To quantify $CD8^+$ cells at single-cell resolution, we developed a digital image approach based on the HALO™ multiplex IHC version 1.2 base algorithm. Color deconvolution was performed both for the nuclear counterstain (RGB 0.179,0.164,0.106) and the DAB product (RGB 0.324,0.482,0.628). For regional analysis, classifiers were trained to identify stromal and tumor regions (the latter defined as regions containing cancer cells), in which the $CD8^+$ T cells were quantified separately. Excluded tumors were defined as all immune-rich tumors (≥10% $CD45^+$ cells in flow analysis) with both a low tumoral $CD8^+$ T cell count, corresponding to 0 or 1+ scoring by an experienced pathologist (average $CD8^+$ T cell count excluded tumors: 45.5 (range 1.96-160.9) $CD8^+/mm^2$, average $CD8^+$ T cell count infiltrated tumors: 564.3 (53.5-1764.7) $CD8^+/mm^2$) and a five-fold higher $CD8^+$ T cell count in the stromal region than in the tumor region (excluded: 526.6 (95.1-1087.9), infiltrated: 1165.2 (106.3-3046.4) $CD8^+/mm^2$).

For quantification of tertiary lymphoid structures, TLS were manually identified and quantified (TLS/mm^2), as based on the presence of B cell (CD20) and T cell (CD3, CD4 and CD8) zones. TLS areas were measured using digital annotation and quantification by HALO™. Lymphoid aggregates <60,000 μm^2 were excluded as described previously[20]. Average TLS areas were obtained by dividing total TLS area by the number of TLS present.

Analysis of secreted mediators:

For analysis of cytokines, chemokines, and cytotoxic mediators, supernatants of PDTF cultures were collected after 48h of culture, unless indicated otherwise. Supernatants were immediately frozen and preserved at -80˚C. Supernatants were thawed on ice, supernatants from each condition were pooled, except for single fragment analyses, and presence of indicated cytokines and chemokines was detected using the LEGENDplex™ Human Th Cytokine, Human Proinflammatory Chemokine, customized Human Proinflammatory Chemokine, and Human CD8/NK panels (all from Biolegend), or using the BLC/CXCL13 Human ELISA Kit (Thermo Fisher) according to the manufacturers' instructions.

Antibody penetration

To measure penetration of exogenously added antibodies into tumor fragments, fluorescently-labeled antibodies recognizing different surface antigens (anti-CD8 AF594 nanobody [218, 1:100, [50]], anti-EpCAM AF647 [9C4, 1:50, Biolegend]) were added to PDTF cultures for the indicated time periods. For subsequent analysis by flow cytometry, PDTFs were processed into single cell suspensions as described above, and samples were counterstained using an anti-CD8 PE antibody [B9.11, 1:100, Beckman Coulter] that binds a non-overlapping epitope. Overlap in signal for the two antibodies was then determined by flow cytometry. For subsequent analysis by immunofluorescence, PDTFs were washed, fixed in 4% paraformaldehyde for 2 hrs and snap frozen in optimal cutting temperature (OCT) compound (CellPath). Sectioning was performed on a microtome-cryostat (CM1950, Leica). Tissue sections were stained with an anti-EpCAM PE antibody [EBA-1, 1:50, BD Biosciences] that binds a non-overlapping epitope and DAPI for nuclear counterstaining. Images were acquired on an Olympus BX63 Apollo fluorescence microscope and analyzed using Image J software version 1.47.

Sorting and in vitro expansion of intratumoral T cells

For isolation of intratumoral T lymphocytes, cryopreserved PDTFs were thawed and digested as described above. Samples were resuspended in 300 µL staining buffer containing the following antibodies: anti-CD45 PerCP Cy5.5 (2D1, 1:100) from Invitrogen; anti-CD3 PE (SK7, 1:50), -CD19 APC (SJ25C1, 1:50), -CD56 APC (HCD56, 1:20), -CD16 APC (3G8, 1:50), -CD11b APC (ICRF44, 1:50), and -CD11c APC (3.9, 1:50) from Biolegend. After 20 min incubation at 4°C, cells were washed twice and cell sorting was performed on a BD FACSAria Fusion SORP cell sorter (BD Biosciences, version 8.0.1). Cells were sorted on SSC-A/FSC-A, FSC-A/FSC-H for singlets and live cells (4',6-diamidino-2-phenylindole, dihydrochloride (DAPI, Sigma-Aldrich) - negative) and T cells, identified as CD45 positive, bulk (CD19, CD56, CD16, CD11b, CD11c) negative and CD3 positive cells. Post-sort sample purity was >98%. Sorted cells were rested at 37 °C in T cell medium (50% AIM-V MED CTS medium (Thermo Fisher) and 50% RPMI 1640 medium, no phenol red (Thermo Fisher), 10% human serum (Sigma), 1% Penicillin-Streptomycin (Roche), 2 mM L-glutamine (Thermo Fisher)). After 2 hrs, cells were expanded in vitro using an excess of irradiated allogeneic feeder cells (4,000 rad) pooled from three healthy donors in T cell medium supplemented with 3,000 IU/mL of IL2 (Peprotech) and 30 ng/mL anti-CD3 (OKT3)[13,15]. From day 7 on, half of the medium was replaced with fresh medium containing IL2 every 2–3 days. Cells were split 1:2 at day 7 and when necessary. From day 15, T cells were further cultured in T cell medium containing 60 IU/mL of IL2 [Preprotech] and cells were cryopreserved at day 18.

Assessment of tumor reactivity

Cryopreserved in vitro expanded intratumoral T lymphocytes were thawed and cultured in T cell medium containing 60 IU/mL of IL2 for 3 days. Subsequently, cells were washed in PBS and fluorescently labeled with 5 µM cell trace violet (CTV, Thermo Fisher). Autologous PDTFs were thawed and digested as described above and cells were rested for 1h at 37°C in complete medium (RPMI 1640 medium (Thermo Fisher), 10% human serum (Sigma), 1% Penicillin-Streptomycin (Roche), 1mM sodium pyruvate (Sigma), 1× MEM non-essential AA (Sigma)).

CTV-labeled T cells (1-2 × 10^5) were cocultured with autologous digest at an effector:tumor cell ratio of 1:1. The percentage of tumor cells in the digests was previously estimated by flow cytometry gating on CD45 negative-FSc high cells. A condition with a blocking anti-HLA class I antibody (hybridoma W6/32, purified in house, 10 μg/ml) was included to determine HLA class I restriction of any observed T cell responses. T cells cultured in the absence of tumor digest, with or without 10 ng/mL PMA (Sigma) and 200 ng/mL ionomycin (Sigma), were used as further controls. After 1h of culture, 1× monensin (BD Biosciences) and 1× brefeldin A (BD Biosciences) were added, and cells were incubated for an additional 16 hrs before analysis of IFN-γ (anti-IFN-γ APC; 4S.B3; 1:50; Biolegend) and TNFα (anti-TNFα PE-Cy7; MAb11; 1:50; BD Biosciences) production by intracellular cytokine staining and flow cytometry. HLA class I expression was detected using anti-HLA ABC FITC (W6/32; 1:50; Biolegend) antibody.

Modulation of anti-PD-1 response

To establish optimal conditions for IFNγR1 blockade and Lck blockade, healthy donor peripheral blood mononuclear cells (PBMCs, Sanquin) were cultured in tumor medium in the absence or presence of either Lck inhibitor (LCKi, CAS 213743-31-8, Merck Millipore) or anti-IFNγ R1 blocking antibody (aIFNγR1, 92101, R&D systems). After 1 (aIFNγR1) or 2 hrs (LCKi) of culture, PBMCs were transferred to a plate coated with anti-CD3 (OKT3, 5 μg/ml)/anti-CD28 (CD28.2, 2 μg/ml) antibodies and cells were cultured in the continued presence of LCKi or aIFNγR1 for 48 hrs. Subsequently, T cell activation and CXCL10 production were assessed by flow cytometry and using the IP-10 Flex Set kit (BD Biosciences).

In PDTF cultures, either 8 μM LCKi or 50 μg/mL aIFNγR1 antibody was added for 2 hrs and 1 h, respectively, prior to ex vivo anti-PD-1 treatment. Samples that were cultured in the absence or presence of anti-PD-1 alone were taken along as control. Cultures were incubated at 37°C and analyzed after 48 hrs.

Statistical analysis

Data are reported as mean ± SD or mean ± SEM, as specified. Statistical significance was determined using the Mann-Whitney test, two-tailed Wilcoxon test, or Kruskal-Wallis test, as indicated (Prism version 8.0e, GraphPad Software). Differences were considered statistically significant if *p<0.05, **p<0.01, ***p<0.001, ****p<0.0001. Only significant p values are displayed. Correlations were evaluated using Spearman's Rank Order correlation and effect sizes were calculated using Hedge's g. All computational analyses were performed in R (version 4.0.2). Unless otherwise specified, experiments were performed without duplicates, because of material restrictions. Data describing reproducibility of cultures are provided in Fig. 2f, Extended Data Fig. 1d-e, Extended Data 3a-d, and Supplementary Fig. 1.

The PDTF response score was developed by first calculating receiver operating characteristic (ROC) curves based on the delta values [anti-PD-1 treated condition minus untreated condition) for each parameter measured in the original cohort. Twelve parameters that were strongly discriminative between responders and non-responders were selected based on the area under the ROC curve (AUROC) (Extended data Fig. 4a,b). For each parameter, a cut-off value was identified aiming for high specificity and sensitivity. This cut-off was used to score each parameter in each sample depending on whether the delta value was above or below the cut-off. Parameters with a specificity >90% were weighted double (Extended data Fig. 4c). The response score was calculated as follows:

$$PDTF\ response\ score = \frac{\sum all\ parameters}{maximal\ score} \times 100$$

Data availability

All relevant flow cytometry, immunohistochemistry, and cytokine/chemokine data are provided as Supplementary data.

Code availability

No custom code was developed. All code used in this study is either specified in the Methods section or available from the corresponding author.

Acknowledgments

We thank Dennis Peters and the NKI-AVL Core Facility for Molecular Pathology & Biobanking for supplying and processing of NKI-AVL Biobank material, the NKI-AVL flow cytometry facility for assistance with sorting and flow cytometric analyses, Lisette Rozeman for assistance with acquisition of clinical data, and all members of the Thommen and Schumacher labs for helpful discussion. This work was supported by a PhD fellowship from the Portuguese Foundation for Science and Technology (SFRH/BD/52042/2012) through the Graduate Program in Basic and Applied Biology (GABBA) to P.V., by KWF (Young investigator grant 12046) and the Swiss National Science Foundation (P300PB_177881) to D.S.T., and by ERC AdG SENSIT (grant agreement No. 742259) to T.N.S..

Author contributions

These authors contributed equally: P.V., M.d.B. and L.M.R.

These authors jointly supervised this work: T.N.S. and D.S.T.

T.N.S. and D.S.T. conceived the study. P.V., L.M.R., A.Z., J.B.A.G.H., T.N.S. and D.S.T. conceived experimental designs. P.V., M.d.B., L.M.R., S.H.H., S.B., M.v.d.B. and P.H. performed experiments. P.V., M.d.B., L.M.R., T.N.S. and D.S.T. analyzed data. A.B., C.U.B., K.J.H., and K.M. contributed to collection of patient samples and data. J.S. and K.M. performed pathological characterization of patient samples. L.M.R., J.S. and K.M. performed digital image analysis. P.V., T.N.S. and D.S.T. wrote the manuscript. All authors reviewed and edited the manuscript.

Competing interests' statement

T.N.S. is advisor for Adaptive Biotechnologies, Allogene Therapeutics, Merus, Neogene Therapeutics, and Scenic Biotech; is a recipient of research support from Merck KgaA; is a stockholder in Allogene

Therapeutics, Merus, Neogene Therapeutics, and Scenic Biotech; and is venture partner at Third Rock Ventures, all outside of the current work. D.S.T. received research funding from Bristol Myers Squibb, outside of the current work. The other authors declare no competing interests.

References

1. Xin Yu, J., *et al.* Trends in clinical development for PD-1/PD-L1 inhibitors. *Nature reviews. Drug discovery* **19**, 163-164 (2020).
2. Yost, K.E., *et al.* Clonal replacement of tumor-specific T cells following PD-1 blockade. *Nature medicine* **25**, 1251-1259 (2019).
3. Wu, T.D., *et al.* Peripheral T cell expansion predicts tumour infiltration and clinical response. *Nature* **579**, 274-278 (2020).
4. Zhang, J., *et al.* Compartmental Analysis of T-cell Clonal Dynamics as a Function of Pathologic Response to Neoadjuvant PD-1 Blockade in Resectable Non-Small Cell Lung Cancer. *Clinical cancer research : an official journal of the American Association for Cancer Research* **26**, 1327-1337 (2020).
5. Strauss, L., *et al.* Targeted deletion of PD-1 in myeloid cells induces antitumor immunity. *Sci Immunol* **5**(2020).
6. Mayoux, M., *et al.* Dendritic cells dictate responses to PD-L1 blockade cancer immunotherapy. *Science translational medicine* **12**(2020).
7. Tumeh, P.C., *et al.* PD-1 blockade induces responses by inhibiting adaptive immune resistance. *Nature* **515**, 568-571 (2014).
8. Amaria, R.N., *et al.* Neoadjuvant immune checkpoint blockade in high-risk resectable melanoma. *Nature medicine* **24**, 1649-1654 (2018).
9. Huang, A.C., *et al.* A single dose of neoadjuvant PD-1 blockade predicts clinical outcomes in resectable melanoma. *Nature medicine* **25**, 454-461 (2019).
10. Neal, J.T., *et al.* Organoid Modeling of the Tumor Immune Microenvironment. *Cell* **175**, 1972-1988 e1916 (2018).
11. Jenkins, R.W., *et al.* Ex Vivo Profiling of PD-1 Blockade Using Organotypic Tumor Spheroids. *Cancer discovery* **8**, 196-215 (2018).
12. Blank, C., *et al.* PD-L1/B7H-1 inhibits the effector phase of tumor rejection by T cell receptor (TCR) transgenic CD8+ T cells. *Cancer Res* **64**, 1140-1145 (2004).
13. Gros, A., *et al.* PD-1 identifies the patient-specific CD8(+) tumor-reactive repertoire infiltrating human tumors. *J Clin Invest* **124**, 2246-2259 (2014).
14. Gros, A., *et al.* Prospective identification of neoantigen-specific lymphocytes in the peripheral blood of melanoma patients. *Nature medicine* **22**, 433-438 (2016).
15. Thommen, D.S., *et al.* A transcriptionally and functionally distinct PD-1(+) CD8(+) T cell pool with predictive potential in non-small-cell lung cancer treated with PD-1 blockade. *Nature medicine* **24**, 994-1004 (2018).
16. Herbst, R.S., *et al.* Predictive correlates of response to the anti-PD-L1 antibody MPDL3280A in cancer patients. *Nature* **515**, 563-567 (2014).
17. Sharma, P. & Allison, J.P. The future of immune checkpoint therapy. *Science* **348**, 56-61 (2015).
18. Hegde, P.S., Karanikas, V. & Evers, S. The Where, the When, and the How of Immune Monitoring for Cancer Immunotherapies in the Era of Checkpoint Inhibition. *Clinical cancer research : an official journal of the American Association for Cancer Research* **22**, 1865-1874 (2016).
19. Galon, J. & Bruni, D. Approaches to treat immune hot, altered and cold tumours with combination immunotherapies. *Nature reviews. Drug discovery* **18**, 197-218 (2019).
20. Sanmamed, M.F., *et al.* Changes in serum interleukin-8 (IL-8) levels reflect and predict response to anti-PD-1 treatment in melanoma and non-small-cell lung cancer patients. *Annals of oncology : official journal of the European Society for Medical Oncology / ESMO* **28**, 1988-1995 (2017).
21. Schalper, K.A., *et al.* Elevated serum interleukin-8 is associated with enhanced intratumor neutrophils and reduced clinical benefit of immune-checkpoint inhibitors. *Nature medicine* **26**, 688-692 (2020).
22. Yuen, K.C., *et al.* High systemic and tumor-associated IL-8 correlates with reduced clinical benefit of PD-L1 blockade. *Nature medicine* **26**, 693-698 (2020).
23. Wherry, E.J., *et al.* Molecular signature of CD8+ T cell exhaustion during chronic viral infection. *Immunity* **27**, 670-684 (2007).
24. Baitsch, L., *et al.* Extended co-expression of inhibitory receptors by human CD8 T-cells depending on differentiation, antigen-specificity and anatomical localization. *PloS one* **7**, e30852 (2012).
25. Thommen, D.S., *et al.* Progression of Lung Cancer Is Associated with Increased Dysfunction of T Cells Defined by Coexpression of Multiple Inhibitory Receptors. *Cancer immunology research* **3**, 1344-1355 (2015).
26. Kurtulus, S., *et al.* Checkpoint Blockade Immunotherapy Induces Dynamic Changes in PD-1(-)CD8(+) Tumor-Infiltrating T Cells. *Immunity* **50**, 181-194 e186 (2019).
27. Siddiqui, I., *et al.* Intratumoral Tcf1(+)PD-1(+)CD8(+) T Cells with Stem-like Properties Promote Tumor Control in Response to Vaccination and Checkpoint Blockade Immunotherapy. *Immunity* **50**, 195-211 e110 (2019).
28. Miller, B.C., *et al.* Subsets of exhausted CD8(+) T cells differentially mediate tumor control and respond to checkpoint blockade. *Nat Immunol* **20**, 326-336 (2019).
29. Sade-Feldman, M., *et al.* Defining T Cell States Associated with Response to Checkpoint Immunotherapy in Melanoma. *Cell* **175**, 998-1013 e1020 (2018).
30. Krishna, S., *et al.* Stem-like CD8 T cells mediate response of adoptive cell immunotherapy against human cancer. *Science* **370**, 1328-1334 (2020).
31. Duhen, T., *et al.* Co-expression of CD39 and CD103 identifies tumor-reactive CD8 T cells in human solid tumors. *Nature communications* **9**, 2724 (2018).

32. Byrne, A.*, et al*. Tissue-resident memory T cells in breast cancer control and immunotherapy responses. *Nature reviews. Clinical oncology* **17**, 341-348 (2020).
33. Edwards, J.*, et al.* CD103(+) Tumor-Resident CD8(+) T Cells Are Associated with Improved Survival in Immunotherapy-Naive Melanoma Patients and Expand Significantly During Anti-PD-1 Treatment. *Clinical cancer research : an official journal of the American Association for Cancer Research* **24**, 3036-3045 (2018).
34. Menares, E.*, et al.* Tissue-resident memory CD8(+) T cells amplify anti-tumor immunity by triggering antigen spreading through dendritic cells. *Nature communications* **10**, 4401 (2019).
35. Ansel, K.M.*, et al.* A chemokine-driven positive feedback loop organizes lymphoid follicles. *Nature* **406**, 309-314 (2000).
36. Gettinger, S.N.*, et al.* A dormant TIL phenotype defines non-small cell lung carcinomas sensitive to immune checkpoint blockers. *Nature communications* **9**, 3196 (2018).
37. Schietinger, A.*, et al.* Tumor-Specific T Cell Dysfunction Is a Dynamic Antigen-Driven Differentiation Program Initiated Early during Tumorigenesis. *Immunity* **45**, 389-401 (2016).
38. Philip, M.*, et al.* Chromatin states define tumour-specific T cell dysfunction and reprogramming. *Nature* **545**, 452-456 (2017).
39. Scheper, W.*, et al.* Low and variable tumor reactivity of the intratumoral TCR repertoire in human cancers. *Nature medicine* **25**, 89-94 (2019).
40. Rizvi, N.A.*, et al.* Cancer immunology. Mutational landscape determines sensitivity to PD-1 blockade in non-small cell lung cancer. *Science* **348**, 124-128 (2015).
41. Helmink, B.A.*, et al.* B cells and tertiary lymphoid structures promote immunotherapy response. *Nature* **577**, 549-555 (2020).
42. Petitprez, F.*, et al.* B cells are associated with survival and immunotherapy response in sarcoma. *Nature* **577**, 556-560 (2020).
43. Cabrita, R.*, et al.* Tertiary lymphoid structures improve immunotherapy and survival in melanoma. *Nature* **577**, 561-565 (2020).
44. Decalf, J., Albert, M.L. & Ziai, J. New tools for pathology: a user's review of a highly multiplexed method for in situ analysis of protein and RNA expression in tissue. *J Pathol* **247**, 650-661 (2019).
45. Rodriques, S.G.*, et al.* Slide-seq: A scalable technology for measuring genome-wide expression at high spatial resolution. *Science* **363**, 1463-1467 (2019).
46. Vickovic, S.*, et al.* High-definition spatial transcriptomics for in situ tissue profiling. *Nature methods* **16**, 987-990 (2019).

References for Online Methods

47. Roederer, M., Nozzi, J.L. & Nason, M.C. SPICE: exploration and analysis of post-cytometric complex multivariate datasets. *Cytometry A* **79**, 167-174 (2011).
48. McInnes, L., Healy, J. & Melville, J. UMAP: Uniform Manifold Approximation and Projection for Dimension Reduction. *arXiv:1802.03426v3 [stat.ML]* (2020).
49. Samusik, N., Good, Z., Spitzer, M.H., Davis, K.L. & Nolan, G.P. Automated mapping of phenotype space with single-cell data. *Nature methods* **13**, 493-496 (2016).
50. Dijkgraaf, F.E.*, et al.* Tissue patrol by resident memory CD8(+) T cells in human skin. *Nat Immunol* **20**, 756-764 (2019).

Figure legends

Figure 1. A human tumor fragment platform that responds to PD-1 blockade. a, Schematic representation of PDTF collection, culture, and analysis strategy. **b**, Heatmap displaying normalized delta values between the anti-PD-1 treated and untreated condition for each parameter (4 T cell activation markers, 13 cytokines, 13 chemokines, n=37 tumors, see Supplementary Table 1). Unsupervised hierarchical clustering identifies two large groups, subsequently termed patient-derived tumor fragment responders (PDTF-R) and non-responders (PDTF-NR). **c**, Principal component analysis (PCA) of the data in **b**, showing separation of samples (top) and parameters (bottom). **d**, PDTF response score (as defined in Extended data Fig. 4) for each tumor, and matched clinical response for tumors from patients treated with PD-1 blockade (CR=complete response, PR=partial response, SD=stable disease, PD=progressive disease). The left graph shows the original cohort (n=37), the right graph shows a validation cohort (n=26, see Supplementary Table 2) with matched clinical data. anti-PD-1 resistant tumors indicate PDTF responses of progressive lesions from patients who received systemic anti-PD-1 treatment before the lesion was surgically removed. Significance was determined by two-sided Fisher's exact test.

Figure 2. Tumor-resident T cells promote response to PD-1 blockade. a, Quantification of activation markers on $CD3^+$ T cells and secreted T cell effector cytokines in PDTFs in the absence or presence of ex vivo PD-1 blockade, as assessed by flow cytometry and bead-based immunoassay, respectively. Shown is an example of a representative responding tumor sample (LU012). **b**, Cytotoxic markers secreted by untreated and anti-PD-1 treated PDTFs displayed separately for PDTF-R and PDTF-NR (n=30, same experiment as in Fig. 1b). *p<0.05, **p<0.01 by two-tailed Wilcoxon test. **c**, Heatmap displaying normalized delta values between the anti-PD-1 treated and untreated condition for each cytotoxic marker. **d**, Effect sizes (calculated as Hedge's g) and p values (by two-tailed Mann-Whitney test) of normalized changes for all cytokine and chemokine parameters and activation markers assessed. **e**, Most significantly increased parameters between untreated and anti-PD-1 treated PDTFs

displayed separately for PDTF-R and PDTF-NR. *p<0.05, **p<0.01, ***p<0.001 by two-tailed Wilcoxon test. **f**, Correlation of log2 fold changes (L2FC, to untreated control) of either two independent PDTF cultures treated with anti-PD-1 (left), or of PDTF cultures treated with anti-PD-1 in absence or presence of IFNγR1 blocking antibody (aIFNγR1, middle), or Lck inhibitor (LCKi, right), respectively. **g**, Correlation of normalized values (z-score) of PDTF cultures that were either untreated or treated with anti-PD-1+LCKi. **h**, Heatmap showing the normalized values of parameters that decreased below steady-state levels in the presence of Lck inhibitor. Note that while we formally cannot exclude an effect through inhibition of Lck in NK/NKT cells, this is considered unlikely because of their low frequencies (150-fold lower than T cells in PDTF-R).

Figure 3. Baseline tumor properties and correlation with immunological response. a, Quantification of major immune subsets within total live cells by flow cytometry. **b**, Quantification of immune infiltrates ($CD45^+$) in immune deserts, immune cell rich non-responding, and immune cell rich responding tumors (n=37 tumors). Shown are mean +/- s.d., **p<0.01, ****p<0.0001 by Kruskal-Wallis test corrected for multiple comparisons. **c**, Strategy for algorithm-based digital area quantification (left) and examples of the two $CD8^+$ T cell distribution patterns observed in immune cell rich tumors (middle). The pie charts indicate fractions of responding and non-responding tumors in excluded and infiltrated TMEs, respectively. **d**, Heatmap of steady-state cytokine and chemokine levels. Data depict normalized values measured after 48 hrs of untreated PDTF culture. Unsupervised clustering was performed within the four defined TME types (desert, excluded, infiltrated PDTF-NR, infiltrated PDTF-R). **e**, Quantification of total steady-state cytokine/chemokine secretion, depicted as the sum of all normalized parameters (n=37 tumors). Shown are mean +/- s.d., *p<0.05, **p<0.01 by Kruskal-Wallis test corrected for multiple comparisons. **f**, Effect sizes (calculated by Hedge's g) and p values (by two-tailed Mann-Whitney test) of steady-state cytokines and chemokines between PDTF-R and PDTF-NR. **g**, Quantifications of the three parameters with the highest statistical significance and

largest effect size in the distinct TME subtypes (n=37 tumors). Shown are mean +/- s.d., *p<0.05, **p<0.01, **p<0.001 by Kruskal-Wallis test corrected for multiple comparisons.

Figure 4. T cell differentiation states across distinct TME types. a, UMAP plots of $CD8^+$ T cells concatenated and equalized from all tumors analyzed (n=34) showing the expression of the indicated immune checkpoints. **b**, Percentage of $CD8^+$ T cells expressing the indicated inhibitory receptors within the distinct TME subtypes (n=34 tumors). Shown are mean +/- s.d., *p<0.05, **p<0.01 by Kruskal-Wallis test corrected for multiple comparisons. **c**, Percentage of $CD8^+$ T cells expressing none, or 1-5 immune checkpoints, as determined by Boolean gating within the distinct TME subtypes (n=34 tumors). Bars indicate the mean. Numbers reflect the fraction of $CD8^+$ T cells co-expressing ≥2 markers. **d**, Flow cytometric analysis showing expression of TCF-1 and CD39 within PD-1^+CD8^+ T cells to identify pre-dysfunctional (TCF-1^+CD39^-) and dysfunctional subsets (TCF-1^-CD39^+), respectively (left). Histograms (right) depict the PD-1 expression level within the two populations indicated in the left plot. **e**, Distribution of TCF-1^+ and $CD39^+$ subsets within the $CD8^+$PD-1^+ T cell population for each tumor in the four different TME subtypes. **f**, Ratio of TCF-1^+ and $CD39^+$ cells within PD-1^+ $CD8^+$ T cells in the distinct TME subtypes.

Figure 5. Differential tumor reactivity in T cell populations in PDTF-R and PDTF-NR tumors. a, UMAP plots of $CD8^+$ T cells in distinct TME subtypes. $CD8^+$ T cells from all tumors analyzed (n=34) were concatenated and the PD-1^+ subset was normalized to 1,600 cells per TME subtype. Clusters reflect subsets with distinct expression of PD-1, CD39, CD103 and TCF-1 (see also Extended data Fig. 11e). T1 (indicated by the dashed line) marks the cluster expressing markers associated with tumor reactivity. **b**, Overlay of PD-1, CD39 and CD103 on the UMAP plot. **c**, Quantification of $CD39^+CD103^+$ cells within $CD8^+$ PD-1^+ T cells or of PD-1^T cells within $CD8^+$ T cells across the distinct TME subtypes (n=34 tumors). PD-1^T expression is defined as a PD-1 expression level above the level found on peripheral blood $CD8^+$ T cells, as described previously[15]. Shown are mean +/- s.d., *p<0.05 by Kruskal-Wallis test corrected

for multiple comparisons. **d**, Representative flow plots depicting IFNγ and TNFα production upon co-culture of expanded $CD8^+$ T cells (TIL) with autologous tumor digest in the absence or presence of an HLA class-I blocking antibody (left). Tumor reactivity is defined as production of either IFNγ, TNFα, or both cytokines. Percentage of $CD8^+$ reactivity in the absence or presence of HLA class-I blocking antibody in five PDTF-R and six PDTF-NR tumors (right).

Figure 6. Tertiary lymphoid structures and their components predict the capacity of human tumors to respond to PD-1 blockade. a-c, Frequency of PD-1^T $CD8^+$ T cells (**a**), PD-1^T $CD4^+$ T cells (**b**), and PD-1^T $CD45^+$ lymphocytes (**c**) within total cells across TME subtypes (n=34 tumors). Shown are mean +/- s.d., *p<0.05, ****p<0.0001 by Kruskal-Wallis test corrected for multiple comparisons. **d**, Example of two tumors out of 33 analyzed, one containing TLS (OV008, top left), one lacking TLS (RE002, top right). TLS are indicated by CD20 staining. Immunohistochemistry stainings of the indicated markers in TLS (bottom). Shown is a region with representative TLS in a lung cancer sample (LU009). **e**, Number and average size of TLS in distinct TME subtypes (n=33 tumors). TLS were identified by CD20 and CD3 staining and quantified and measured by digital analysis. Lymphoid aggregates <60,000 μm^2 were excluded, as described previously[42]. Shown are mean +/- s.d., *p<0.05, **p<0.01, ***p<0.001 by Kruskal-Wallis test corrected for multiple comparisons. **f**, Quantification of B cells within total live cells across TME subtypes (n=37 tumors). Shown are mean +/- s.d., *p<0.05, ***p<0.001 by Kruskal-Wallis test corrected for multiple comparisons. **g**, Predictive potential of indicated markers defined by the area under the receiver operator curve (AUROC).

Extended Data Figure 1. Development and validation of ex vivo patient-derived tumor fragment (PDTF) cultures. a, Macroscopic image of a lung tumor processed into PDTFs. PDTFs from distinct tumor regions were mixed to offset the effects of tumor heterogeneity and were immediately cryopreserved. **b**, Flow plots showing total live cells and T cell ($CD45^+CD3^+$), non-T cell ($CD45^+CD3^-$) and

non-immune cell subsets ($CD45^-CD3^-$) of digested PDTFs and culture supernatant after 48 hrs of culture in absence of the matrix (left), and quantification of these subsets in three tumor samples (right). **c**, Viability and lymphocyte efflux (measured by manual counting of cells in culture supernatants) of PDTFs cultured for 48 hrs in either medium, collagen, or complete matrix (top), and quantification of T cells ($CD45^+CD3^+$), non-T cells ($CD45^+CD3^-$) and non-immune cells ($CD45^-CD3^-$) in PDTFs cultured in these conditions. Representative flow plots (middle) and mean and s.e.m. of three PDTF cultures (bottom) are depicted. **d**, Correlation matrix depicting the Spearman co-efficient (left) and heatmap (right) of cytokine/chemokine measurements performed at 24, 36, and 48 hrs of PDTF cultures for four different tumors. The log2 fold change (L2FC) relative to the matching 12h sample is depicted. **e**, Antibody penetration assays, comparing overlap in fluorescence of two antibodies recognizing different epitopes of the same target. Antibodies were either added to the culture at indicated time points, or were used for subsequent staining after tissue processing into single cell suspensions (anti-CD8, left), or tissue slides (anti-EpCAM, right). Shown is one of 4 independent experiments. **f**, Correlation matrix depicting the Spearman co-efficient (left) and heatmap (right) of cytokine/chemokine measurements at 48 hrs in two parallel cultures from each tumor for six different tumors. Normalized values for each parameter are depicted.

Extended Data Figure 2. Ex vivo treatment of PDTFs with anti-PD-1. a, Representative flow plot (LU019) and correlation of PD-1 expression analyzed directly ex vivo and after 48 hrs of culture on either $CD8^+$ (left) or $CD4^+$ (right) T cells (n=37). **b**, T cell activation (LU019) and cytokine/chemokine secretion upon either anti-PD-1 or a matching human IgG4 (S228P) isotype control treatment. The bar graph indicates the fold change compared to the untreated culture. **c**, Comparison of ex vivo anti-PD-1 treatment for 24 hrs and 48 hrs, expressed as log2 fold change (L2FC) relative to untreated PDTFs (n=3). **d**, Study cohort overview.

Extended Data Figure 3. Reproducibility of PDTF responses. a, T cell activation and cytokine/chemokine profiling upon PD-1 blockade in two independently performed PDTF cultures for five responding tumors and one non-responding tumor. Normalized delta values between the treated and the untreated condition are depicted. **b**, Immunological responses of individual tumor fragments. The fold change and p value for each parameter of each untreated or anti-PD-1 treated fragment was calculated against the mean of all untreated fragments (n=3 PDTF-R tumors). **c**, Fold change and p value for each parameter of averaged anti-PD-1 treated versus untreated PDTFs from the same experiment as in (**b**). Significance in **b** and **c** were calculated for each parameter and comparison by unpaired two-sample t test with two-stage linear step-up procedure of Benjamini, Krieger and Yekutieli. **d**, Violin plots showing the range of response scores (as defined in Extended data Fig. 4) for 100 randomly selected combinations of 1-7 individual tumor fragments for both the untreated and anti-PD-1 treated condition. Data are derived from the experiment shown in (**b**). The dashed line indicates the response score when using data from all 8 tumor fragments, as done in standard PDTF cultures, the grey shaded area indicates a positive response score. Note that the data also emphasize heterogeneity in response capacity – but not response type - of individual tumor fragments of a given tumor (**b**).

Extended Data Figure 4. Development of the PDTF response score. a, Potential of indicated markers defined by the area under the receiver operator curve (AUROC) to discriminate between anti-PD-1 responsive and non-responsive tumors. **b**, ROC curves of the 12 parameters selected for the score. As a comparison, plots for two parameters with no discriminative value (IL8 and IL17F) are depicted. **c**, Weighting of the twelve parameters used in the score. **d**, PDTF response scores for 11 tumors for which two or three lesions from distinct localizations were tested (Supplementary Table 3). Tumors with concordant (8/11) and discordant (3/11) responses are indicated. **e**, PDTF response score and matched clinical response for lesions derived from either lymph node metastases (left, n=27) or

primary tumors (P)/distant metastases (M) (right, n=18). Significance was determined by Fisher's exact test.

Extended Data Figure 5. T cell activation upon ex vivo PD-1 blockade in PDTF-R and PDTF-NR tumors. **a**, Expression of T cell activation markers in $CD4^+$ T cells (top) and $CD8^+$ T cells (bottom) from untreated or anti-PD-1 treated PDTF cultures, as assessed by flow cytometry. Data are from the same responding tumor sample as in Fig. 2a (LU012). **b**, Expression of T cell activation markers in $CD3^+$ T cells and secretion of T cell effector cytokines in PDTFs that were either untreated, treated with PD-1 blockade, or treated with anti-CD3 antibodies, as assessed by flow cytometry and bead-based immunoassay, respectively. Data from a representative infiltrated non-responding tumor sample (LU010) are depicted. **c**, Quantification of CD137 and OX40 expression on $CD3^+$ T cells in PDTFs that were either untreated, treated with PD-1 blockade, or treated with anti-CD3 antibodies (n=10 PDTF-NRs). *p<0.05, **p<0.01 by Kruskal-Wallis test corrected for multiple comparisons.

Extended Data Figure 6. Immunological responses upon ex vivo PD-1 blockade. Comparison of additional parameters assessed in untreated and anti-PD-1 treated PDTFs that are not depicted in Figure 2c. Values are displayed separately for PDTF-R and PDTF-NR. *p<0.05, **p<0.01, ***p<0.001 by two-tailed Wilcoxon test.

Extended Data Figure 7. Modulation of the anti-PD-1 response by LCK inhibition or IFNγ receptor blockade. a-**b**, Titration of Lck inhibitor (LCKi) (**a**) and IFNγ receptor 1 blocking antibody (aIFNγR1) (**b**) in PBMCs stimulated with anti-CD3/anti-CD28 for 48 hrs. LCKi was added 2 hrs and aIFNγR1 1 h before PD-1 blockade at the indicated concentrations. The differential inhibition of CD137 expression on $CD3^+$ T cells and CXCL10 secretion reflect interference at the level of T cell activation (LCKi), or downstream, at the level of IFNγ-induced gene expression (aIFNγR1). Viability was comparable for both compounds and at all dosing levels. Shown are 2 independent experiments. Bars and error bars indicate mean +

s.e.m. **c**, Flow plot depicting blockade of the IFNγR1 in the presence of aIFNγR1 during culture, as measured using a fluorescently labeled aIFNγR1 antibody that binds to the same epitope. **d**, Flow plots depicting activation of $CD8^+$ T cells, as measured by CD137 expression, and $CD4^+$ T cells, as measured by OX40 expression, in PDTFs that were either uncultured or treated with anti-PD-1, anti-PD-1+aIFNγR1 or anti-PD-1+LCKi for 48 hrs. One representative example of 8 PDTF cultures is depicted. **e**, T cell activation and cytokine/chemokine profiling of 8 PDTF-R tumors treated with anti-PD-1, anti-PD-1+αIFNgR1, or anti-PD-1+LCKi for 48 hrs. Data are expressed as log2 fold change (L2FC) relative to the untreated condition.

Extended data Figure 8. Immune composition of PDTF-R and PDTF-NR tumors. a, Flow plots depicting the gating strategy and tSNE clustering of immune subsets. **b**, Quantification of indicated immune cell subsets within total immune cells ($CD45^+$) for the four distinct TME subtypes (desert, excluded, infiltrated non-responders, and infiltrated-responders, n=37). Shown are mean +/- s.d., *p<0.05, **p<0.01 by Kruskal-Wallis test. **c**, Correlation between the percentage of $CD8^+$ T cells quantified by either flow cytometry or IHC in matched samples (n=35). Significance was determined by linear regression analysis. **d**, Digital quantification of $CD8^+$ T cells in intratumoral and stromal regions displayed per tumor type (n=35). Bars and error bars indicate mean + s.d..

Extended Data Figure 9. Steady-state cytokine and chemokine profiles. Quantification of additional parameters assessed in untreated PDTFs after 48 hrs of culture (n=37) that are not depicted in Figure 3g. Values are displayed separately for desert, excluded, infiltrated PDTF-NR and infiltrated PDTF-R tumors. Shown are mean +/- s.d., *p<0.05, **p<0.01 by Kruskal-Wallis test corrected for multiple comparisons.

Extended Data Figure 10. T cell differentiation states and tumor reactivity across distinct TME types. **a**, SPICE analysis[47] visualizing the co-expression of distinct immune checkpoints on $CD8^+$ T cells within

the TME subtypes (as indicated by the pie arc). Means of all tumors per TME subtype (Desert, n=10; Excluded, n=5; Infiltrated PDTF-NR, n=6; Infiltrated PDTF-R, n=13) are depicted. **b-d**, Quantification of TCF-1, CD39, and CD103 expression on PD-1^{+}CD8^{+} T cells by flow cytometry (n=34). Shown are mean +/- s.d., $^{**}p<0.01$ by Kruskal-Wallis test corrected for multiple comparisons. **e**, Violin plots showing the expression of PD-1, CD39, CD103, and TCF-1 in the clusters defined in Figure 5a. **f**, Detection of HLA class-I on total live cells in the absence or presence of an HLA I blocking antibody. **g**, Tumor reactivity (measured as production of either IFNγ, TNFα, or both) within expanded CD4^{+} T cells in the absence or presence of tumor digest for five PDTF-R and six PDTF-NR tumors.

Supplementary Figure 1. PDTF culture maintenance. a-c, Flow plots showing CD137 expression on CD3+ T cells (**a**) and heatmaps indicating cytokine and chemokine secretion and T cell activation in untreated (**b**, log2-transformed data) and stimulated (**c**, log2 fold change to untreated) PDTFs that were either cultured in matrix or in medium alone. OV014 was stimulated with aCD3/aCD28, RE027 and OV018 were stimulated with aCD3 only. **d**, Correlation matrix depicting the Spearman co-efficient of cytokine/chemokine measurements and activation markers at 48 hrs in unstimulated and stimulated PDTFs that were either cultured in matrix or in medium. **e-h**, Heatmaps showing cytokine/chemokine secretion and T cell activation in untreated (**e**, log2-transformed data) and aCD3/aCD28 stimulated (**f**, log2 fold change to untreated) PDTFs that were cultured in different glucose concentrations (DMEM high 4,500 mg/L, DMEM low 1,000 mg/L, RPMI1640 2,000 mg/L). **g**, Correlation matrix depicting the Spearman co-efficient of cytokine/chemokine measurements and activation markers at 48 hrs in unstimulated and stimulated PDTFs that were cultured in different glucose concentrations. **h**, Heatmap showing cytokine/chemokine secretion and T cell activation in aCD3/aCD28 stimulated (log2 fold change to untreated) PDTFs that were cultured in different fetal bovine serum (FBS) or human serum (HS) concentrations.

Supplementary Figure 2. Comparison of infiltrated PDTF-NR and PDTF-R tumors. a, Effect size (calculated by Hedge's g) and *p* values (by two-tailed Mann-Whitney test) of differences in steady-state cytokine and chemokine production between infiltrated PDTF-R and PDTF-NR. **b**, Most differentially expressed cytokines and chemokines between infiltrated PDTF-R and PDTF-NR (n=21 tumors). Shown are mean +/- s.d., *p<0.05, **p<0.01, ****p<0.0001 by two-tailed Mann-Whitney test.

Supplementary Figure 3. Analysis of infiltrating myeloid subsets. a, Quantification of the myeloid infiltrate within total immune cells ($CD45^+$) for the four distinct TME subtypes (n=32). Shown are mean +/- s.d., **p<0.01 by Kruskal-Wallis test corrected for multiple comparisons. **b**, UMAP clustering of lymphoid, myeloid, fibroblast and endothelial cell subsets (left). Overlay plots indicating expression of the markers used for assessment of myeloid cells. **c**, Depiction of myeloid clusters on the UMAP plot. **d**, Normalized expression of different myeloid markers on the nine identified myeloid clusters. **e**, Quantification of the myeloid clusters within total immune cells ($CD45^+$) in each tumor. **f**, Pie charts indicating the distribution of myeloid clusters per TME subgroup. **g**, Quantification of myeloid clusters in all TME groups. *p<0.05 by Kruskal-Wallis test corrected for multiple comparisons.

Supplementary Figure 4. Gating strategy and marker expression. a, Gating strategy used for all flow cytometry experiments and for sorting. **b**, Flow plots showing the expression of all markers used to identify major immune cell subsets either within CD3+ or CD3- subsets. **c**, Flow plots showing the expression of inhibitory receptors gated on CD8+ T cells. **d**, Flow plots showing the expression of myeloid markers gated within the Lin- population.

Tables

Supplementary Table 1.

Supplementary Table 2.

Supplementary Table 3.

Supplementary Data:

Supplementary Data 1. PDTF culture setup and validation

Supplementary Data 2. PDTF cultures with ex vivo PD-1 blockade and perturbations

Supplementary Data 3. Immune composition and tumor microenvironment analyses

Figure 1

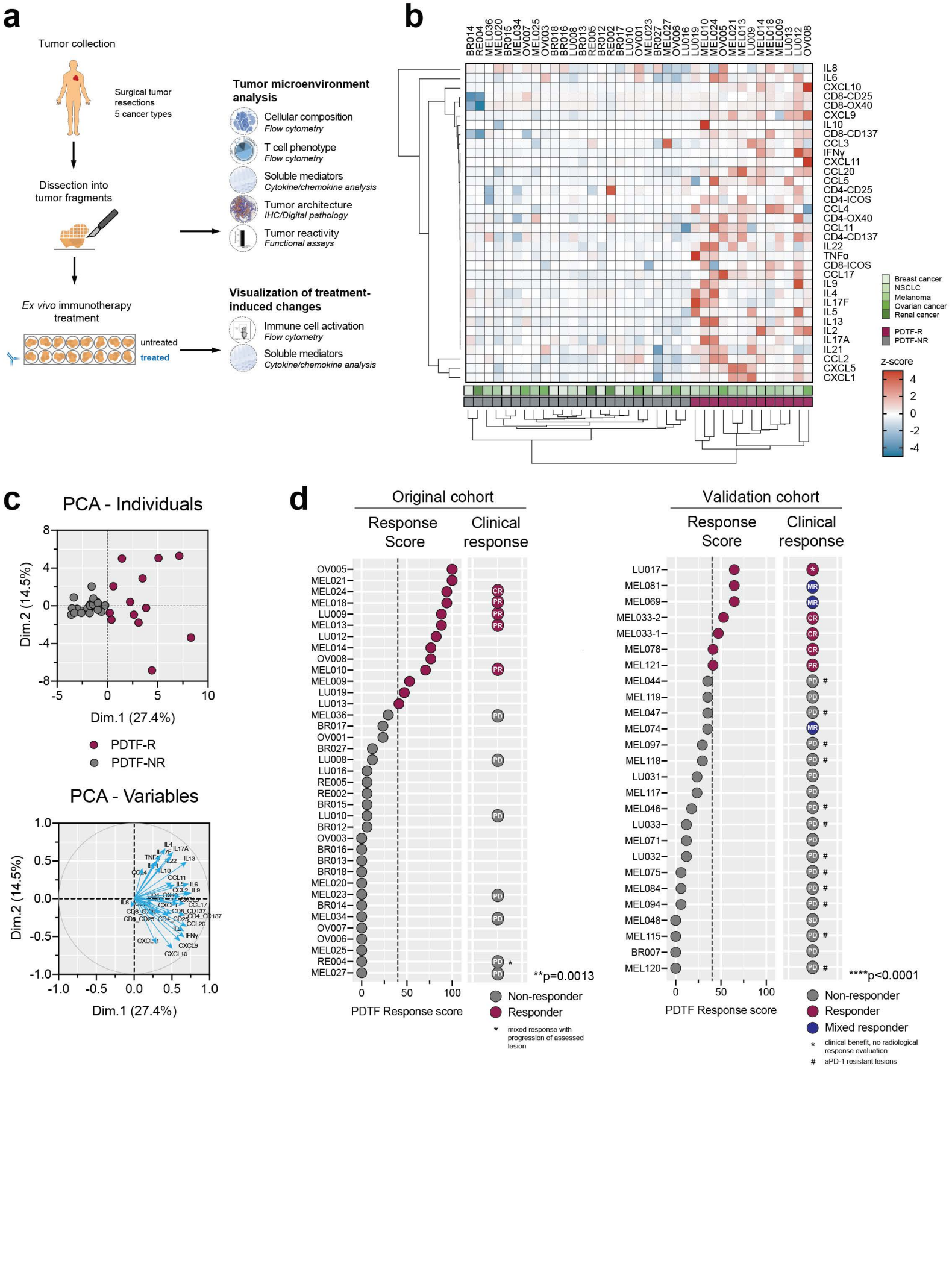
a
Tumor collection
Surgical tumor resections
5 cancer types
Dissection into tumor fragments
Ex vivo immunotherapy treatment
untreated
treated
Tumor microenvironment analysis
Cellular composition
Flow cytometry
T cell phenotype
Flow cytometry
Soluble mediators
Cytokine/chemokine analysis
Tumor architecture
IHC/Digital pathology
Tumor reactivity
Functional assays
Visualization of treatment-induced changes
Immune cell activation
Flow cytometry
Soluble mediators
Cytokine/chemokine analysis
b
BR014 RE004 MEL036 MEL020 BR015 MEL034 OV007 MEL025 OV003 BR018 BR016 LU008 BR013 RE005 BR012 RE002 BR017 LU010 OV001 MEL023 BR027 MEL027 OV006 LU016 LU019 MEL010 MEL024 OV005 MEL021 MEL013 LU009 MEL014 MEL018 MEL009 LU013 LU012 OV008
IL8 IL6 CXCL10 CD8-CD25 CD8-OX40 CXCL9 IL10 CD8-CD137 CCL3 IFNγ CXCL11 CCL20 CCL5 CD4-CD25 CD4-ICOS CCL4 CD4-OX40 CCL11 CD4-CD137 IL22 TNFα CD8-ICOS CCL17 IL9 IL4 IL17F IL5 IL13 IL2 IL17A IL21 CCL2 CXCL5 CXCL1
Breast cancer
NSCLC
Melanoma
Ovarian cancer
Renal cancer
PDTF-R
PDTF-NR
z-score
4
2
0
-2
-4
c
PCA - Individuals
Dim.2 (14.5%)
Dim.1 (27.4%)
PDTF-R
PDTF-NR
PCA - Variables
Dim.2 (14.5%)
Dim.1 (27.4%)
d
Original cohort
Response Score
Clinical response
PDTF Response score
**p=0.0013
Non-responder
Responder
* mixed response with progression of assessed lesion
Validation cohort
Response Score
Clinical response
PDTF Response score
****p<0.0001
Non-responder
Responder
Mixed responder
* clinical benefit, no radiological response evaluation
# aPD-1 resistant lesions

Figure 2

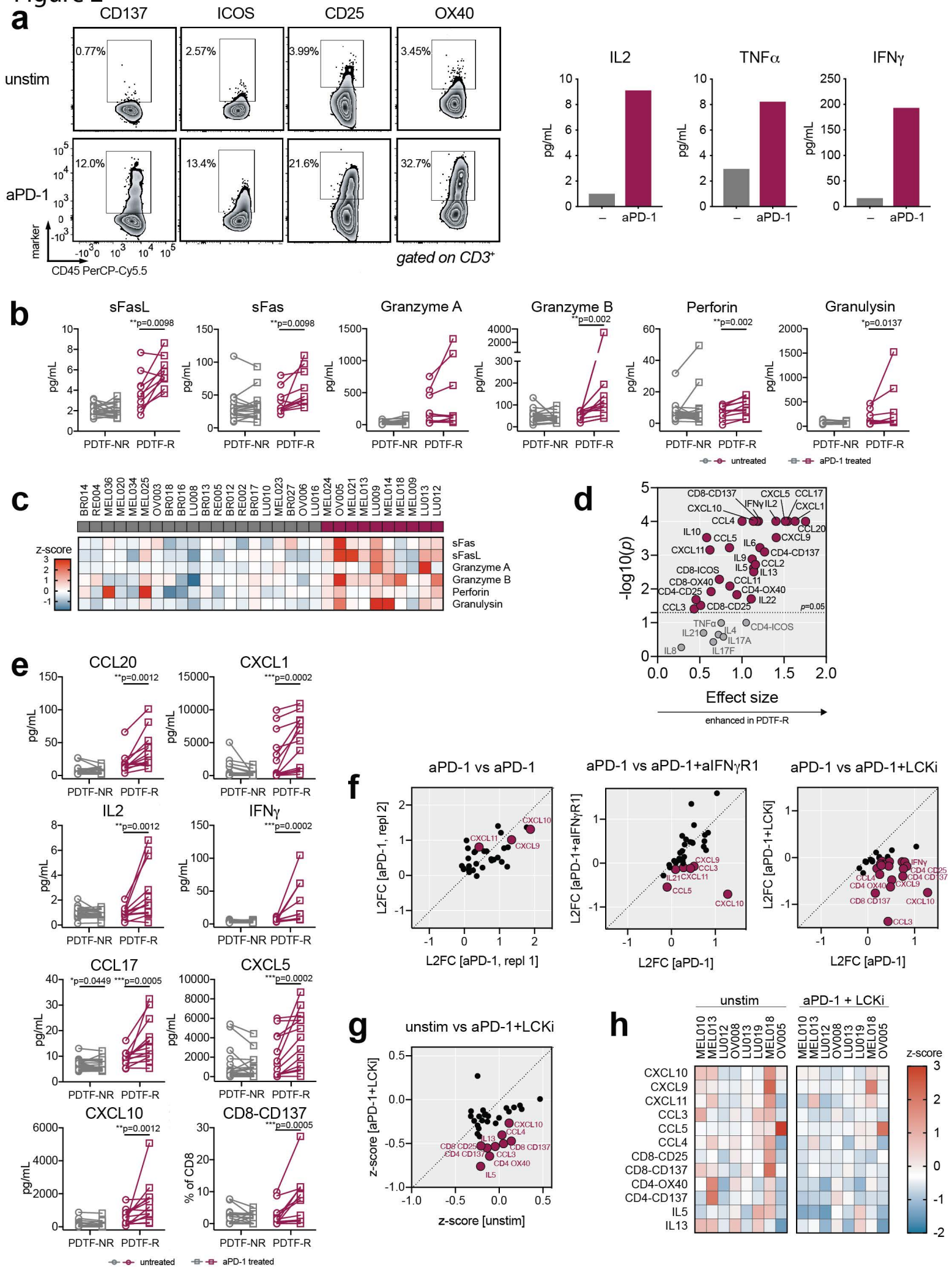
a
CD137
ICOS
CD25
OX40
unstim
aPD-1
0.77%
2.57%
3.99%
3.45%
12.0%
13.4%
21.6%
32.7%
marker
CD45 PerCP-Cy5.5
gated on CD3+
IL2
TNFα
IFNγ
pg/mL
–
aPD-1
b
sFasL
sFas
Granzyme A
Granzyme B
Perforin
Granulysin
**p=0.0098
**p=0.0098
**p=0.002
**p=0.002
*p=0.0137
PDTF-NR
PDTF-R
untreated
aPD-1 treated
c
BR014
RE004
MEL036
MEL020
MEL034
MEL025
OV003
BR018
BR016
LU008
BR013
RE005
BR012
RE002
BR017
LU010
MEL023
BR027
OV006
LU016
MEL024
OV005
MEL021
MEL013
LU009
MEL014
MEL018
MEL009
LU013
LU012
z-score
sFas
sFasL
Granzyme A
Granzyme B
Perforin
Granulysin
d
-log10(p)
Effect size
enhanced in PDTF-R
p=0.05
CD8-CD137
CXCL5
CCL17
CXCL10
IFNγ
IL2
CXCL1
CCL4
CCL20
IL10
CCL5
IL6
CXCL9
CXCL11
CD4-CD137
IL9
CCL2
CD8-ICOS
IL5
IL13
CD8-OX40
CCL11
CD4-CD25
CD4-OX40
IL22
CCL3
CD8-CD25
TNFα
CD4-ICOS
IL21
IL4
IL17A
IL8
IL17F
e
CCL20
CXCL1
IL2
IFNγ
CCL17
CXCL5
CXCL10
CD8-CD137
**p=0.0012
***p=0.0002
*p=0.0449
***p=0.0005
pg/mL
% of CD8
PDTF-NR
PDTF-R
untreated
aPD-1 treated
f
aPD-1 vs aPD-1
aPD-1 vs aPD-1+aIFNγR1
aPD-1 vs aPD-1+LCKi
L2FC [aPD-1, repl 2]
L2FC [aPD-1, repl 1]
L2FC [aPD-1+aIFNγR1]
L2FC [aPD-1]
L2FC [aPD-1+LCKi]
CXCL10
CXCL11
CXCL9
CCL3
IL21
CCL5
IFNγ
CD4 CD25
CD4 CD137
CCL4
CD4 OX40
CXCL9
CD8 CD137
g
unstim vs aPD-1+LCKi
z-score [aPD-1+LCKi]
z-score [unstim]
CXCL10
CCL4
IL13
CD8 CD25
CD8 CD137
CD4 CD137
CCL3
CD4 OX40
IL5
h
unstim
aPD-1 + LCKi
MEL010
MEL013
LU012
OV008
LU013
LU019
MEL018
OV005
z-score
CXCL10
CXCL9
CXCL11
CCL3
CCL5
CCL4
CD8-CD25
CD8-CD137
CD4-OX40
CD4-CD137
IL5
IL13

Figure 3

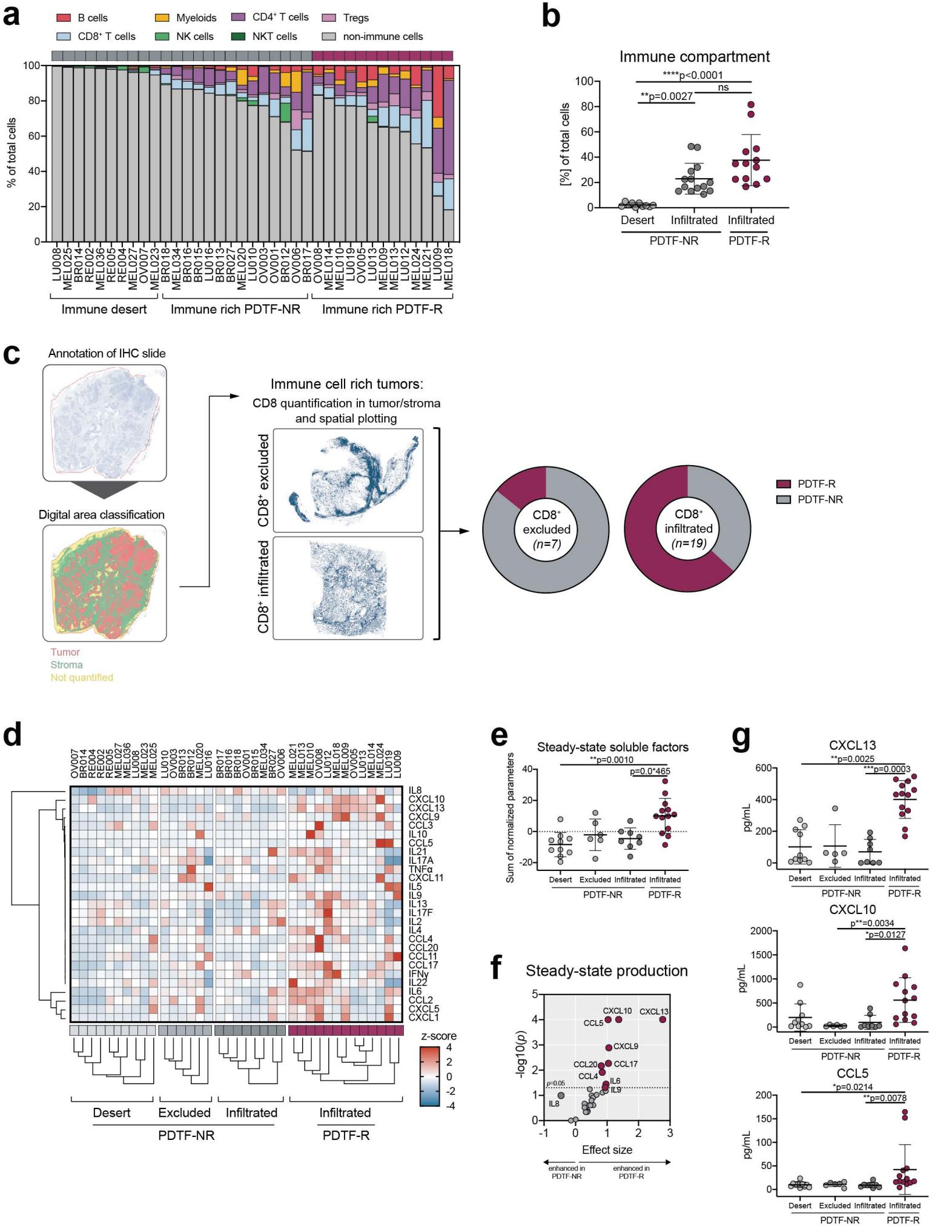
a
B cells
Myeloids
CD4+ T cells
Tregs
CD8+ T cells
NK cells
NKT cells
non-immune cells
% of total cells
Immune desert
Immune rich PDTF-NR
Immune rich PDTF-R
b
Immune compartment
****p<0.0001
**p=0.0027
ns
[%] of total cells
Desert
Infiltrated
Infiltrated
PDTF-NR
PDTF-R
c
Annotation of IHC slide
Digital area classification
Tumor
Stroma
Not quantified
Immune cell rich tumors:
CD8 quantification in tumor/stroma
and spatial plotting
CD8+ excluded
CD8+ infiltrated
CD8+ excluded (n=7)
CD8+ infiltrated (n=19)
PDTF-R
PDTF-NR
d
IL8
CXCL10
CXCL13
CXCL9
CCL3
IL10
CCL5
IL21
IL17A
TNFα
CXCL11
IL5
IL9
IL13
IL17F
IL2
IL4
CCL4
CCL20
CCL11
CCL17
IFNγ
IL22
IL6
CCL2
CXCL5
CXCL1
z-score
Desert
Excluded
Infiltrated
Infiltrated
PDTF-NR
PDTF-R
e
Steady-state soluble factors
**p=0.0010
p=0.0*465
Sum of normalized parameters
Desert
Excluded
Infiltrated
Infiltrated
PDTF-NR
PDTF-R
f
Steady-state production
-log10(p)
Effect size
enhanced in PDTF-NR
enhanced in PDTF-R
p=0.05
g
CXCL13
**p=0.0025
***p=0.0003
CXCL10
p**=0.0034
*p=0.0127
CCL5
*p=0.0214
**p=0.0078
pg/mL

Figure 4

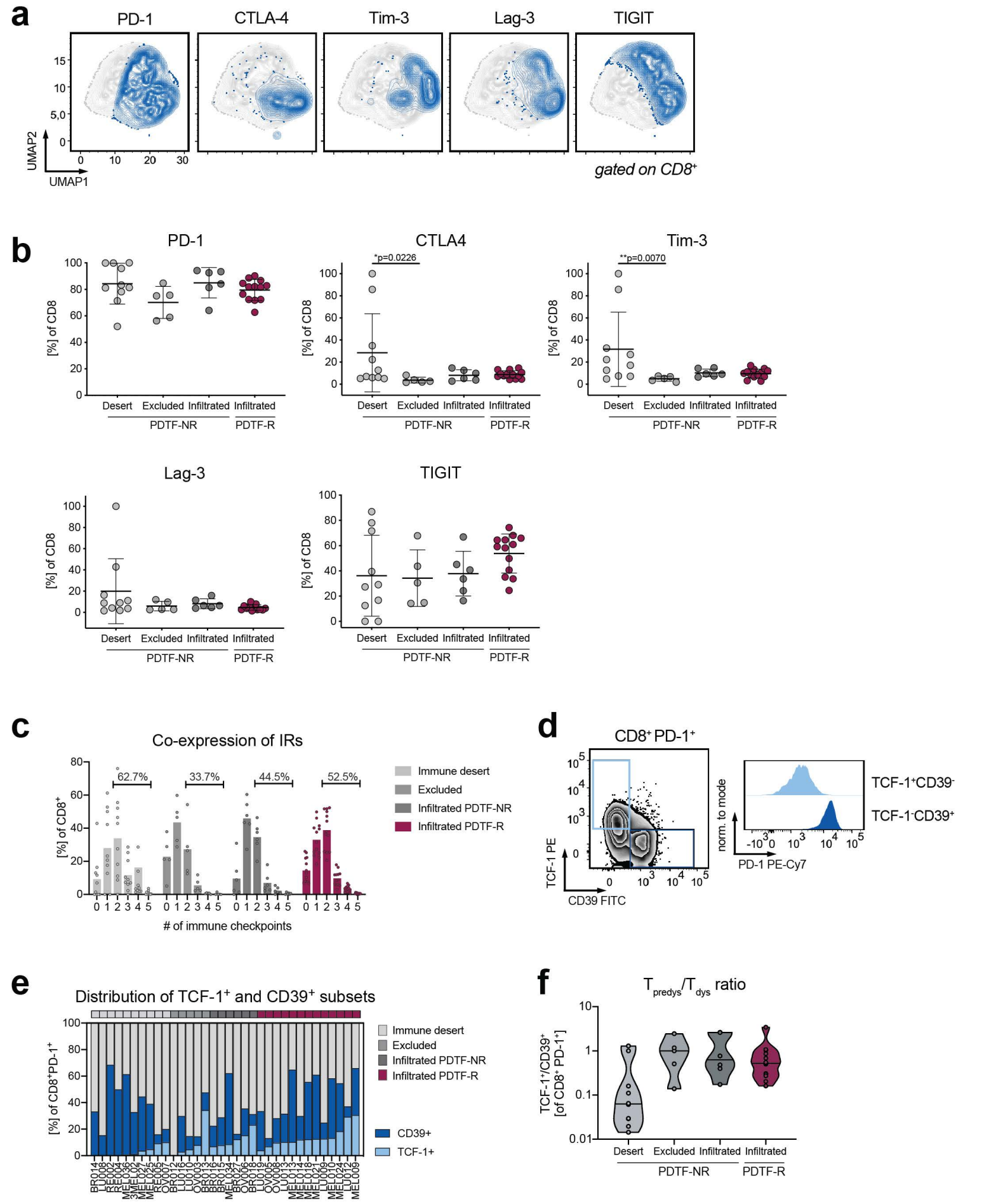
a
PD-1
CTLA-4
Tim-3
Lag-3
TIGIT
UMAP2
UMAP1
gated on CD8+
b
PD-1
CTLA4
Tim-3
Lag-3
TIGIT
[%] of CD8
*p=0.0226
**p=0.0070
Desert
Excluded
Infiltrated
Infiltrated
PDTF-NR
PDTF-R
c
Co-expression of IRs
[%] of CD8+
62.7%
33.7%
44.5%
52.5%
# of immune checkpoints
Immune desert
Excluded
Infiltrated PDTF-NR
Infiltrated PDTF-R
d
CD8+ PD-1+
TCF-1 PE
CD39 FITC
norm. to mode
PD-1 PE-Cy7
TCF-1+CD39-
TCF-1-CD39+
e
Distribution of TCF-1+ and CD39+ subsets
[%] of CD8+PD-1+
CD39+
TCF-1+
f
Tpredys/Tdys ratio
TCF-1+/CD39+ [of CD8+ PD-1+]

Figure 5

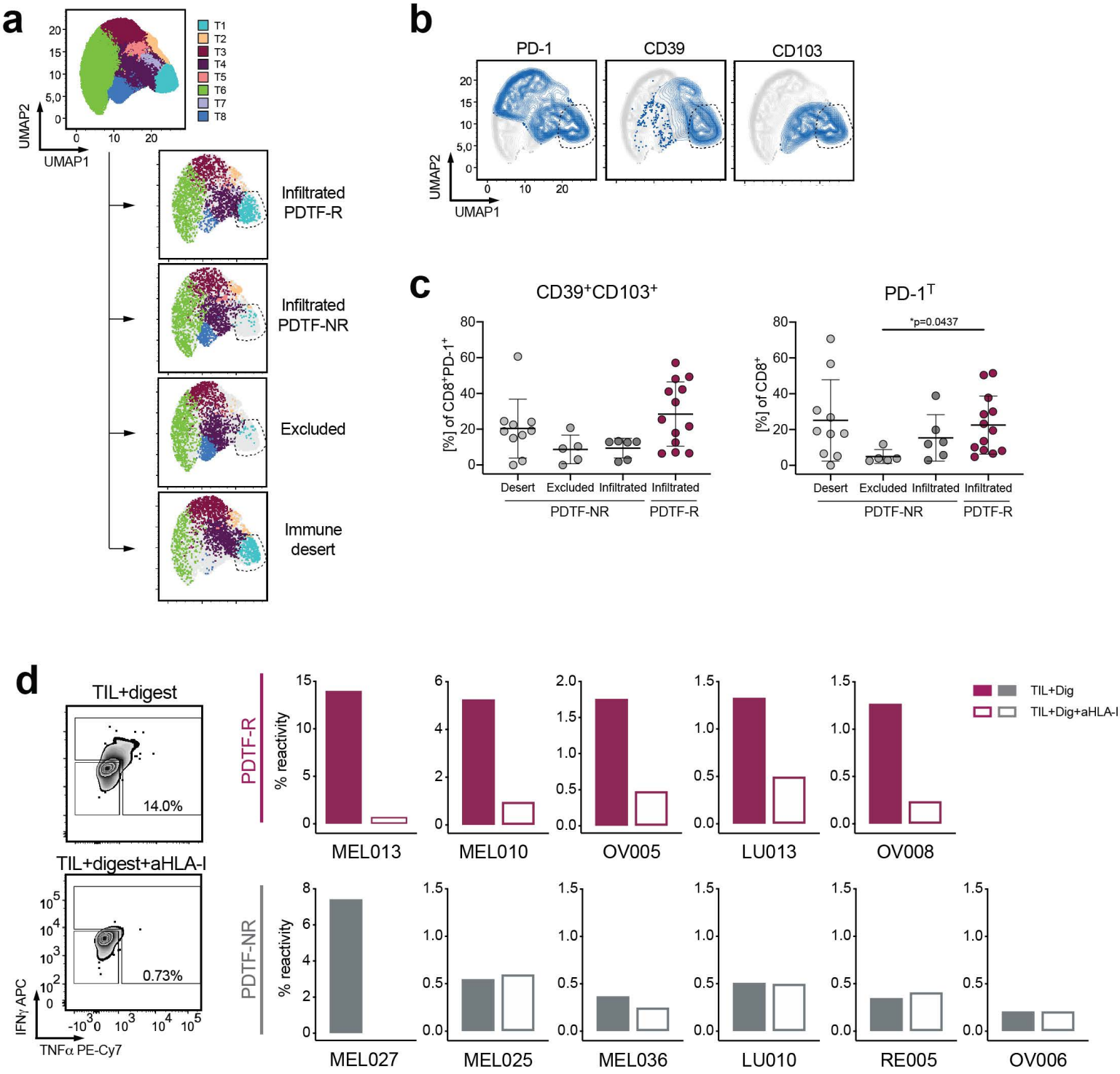
a
T1
T2
T3
T4
T5
T6
T7
T8
UMAP2
UMAP1
Infiltrated PDTF-R
Infiltrated PDTF-NR
Excluded
Immune desert
b
PD-1
CD39
CD103
UMAP2
UMAP1
c
CD39+CD103+
[%] of CD8+PD-1+
Desert
Excluded
Infiltrated
Infiltrated
PDTF-NR
PDTF-R
PD-1T
*p=0.0437
[%] of CD8+
d
TIL+digest
14.0%
TIL+digest+aHLA-I
0.73%
IFNγ APC
TNFα PE-Cy7
PDTF-R
% reactivity
TIL+Dig
TIL+Dig+aHLA-I
MEL013
MEL010
OV005
LU013
OV008
PDTF-NR
MEL027
MEL025
MEL036
LU010
RE005
OV006

Figure 6

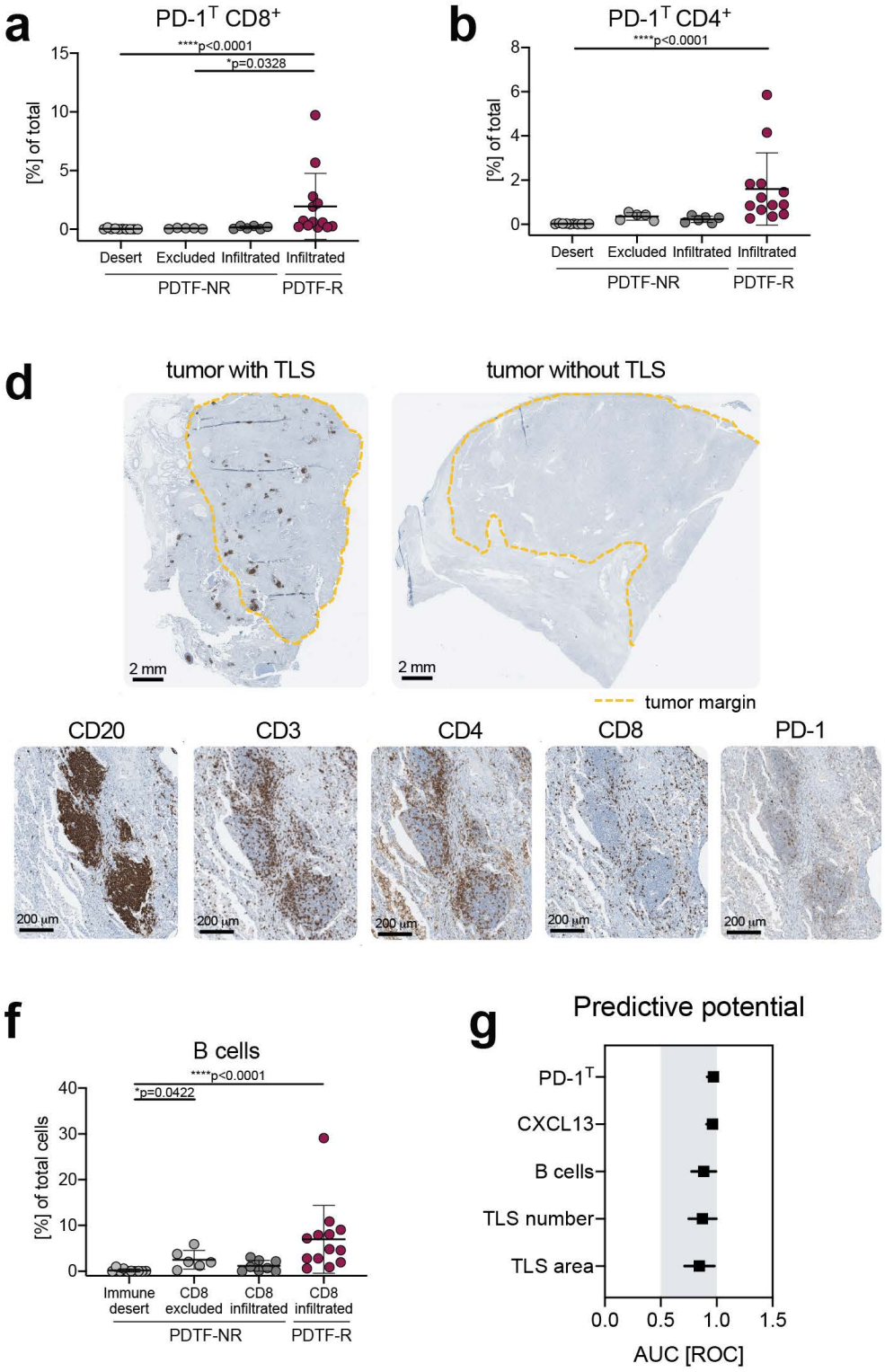
a
PD-1T CD8+
****p<0.0001
*p=0.0328
[%] of total
Desert
Excluded
Infiltrated
Infiltrated
PDTF-NR
PDTF-R
b
PD-1T CD4+
****p<0.0001
c
PD-1T lymphocytes
****p<0.0001
d
tumor with TLS
tumor without TLS
2 mm
tumor margin
CD20
CD3
CD4
CD8
PD-1
200 µm
e
TLS number
p=0.0811
***p=0.0009
TLS per mm2 area
Immune desert
CD8 excluded
CD8 infiltrated
CD8 infiltrated
TLS size
*p=0.0378
**p=0.0035
Average TLS area (mm2)
f
B cells
****p<0.0001
*p=0.0422
[%] of total cells
g
Predictive potential
PD-1T
CXCL13
B cells
TLS number
TLS area
AUC [ROC]

Extended Data Figure 1

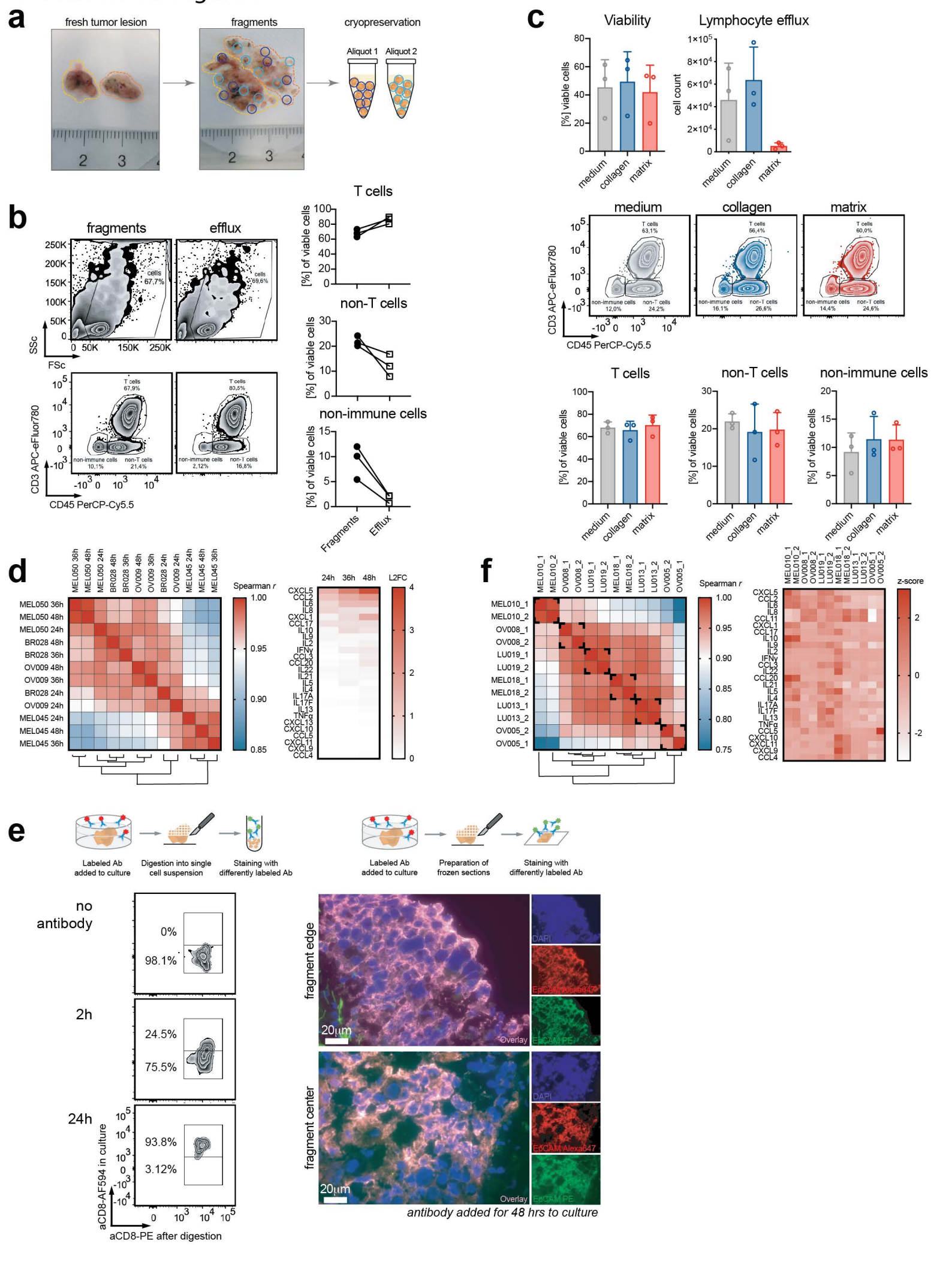

Extended Data Figure 2

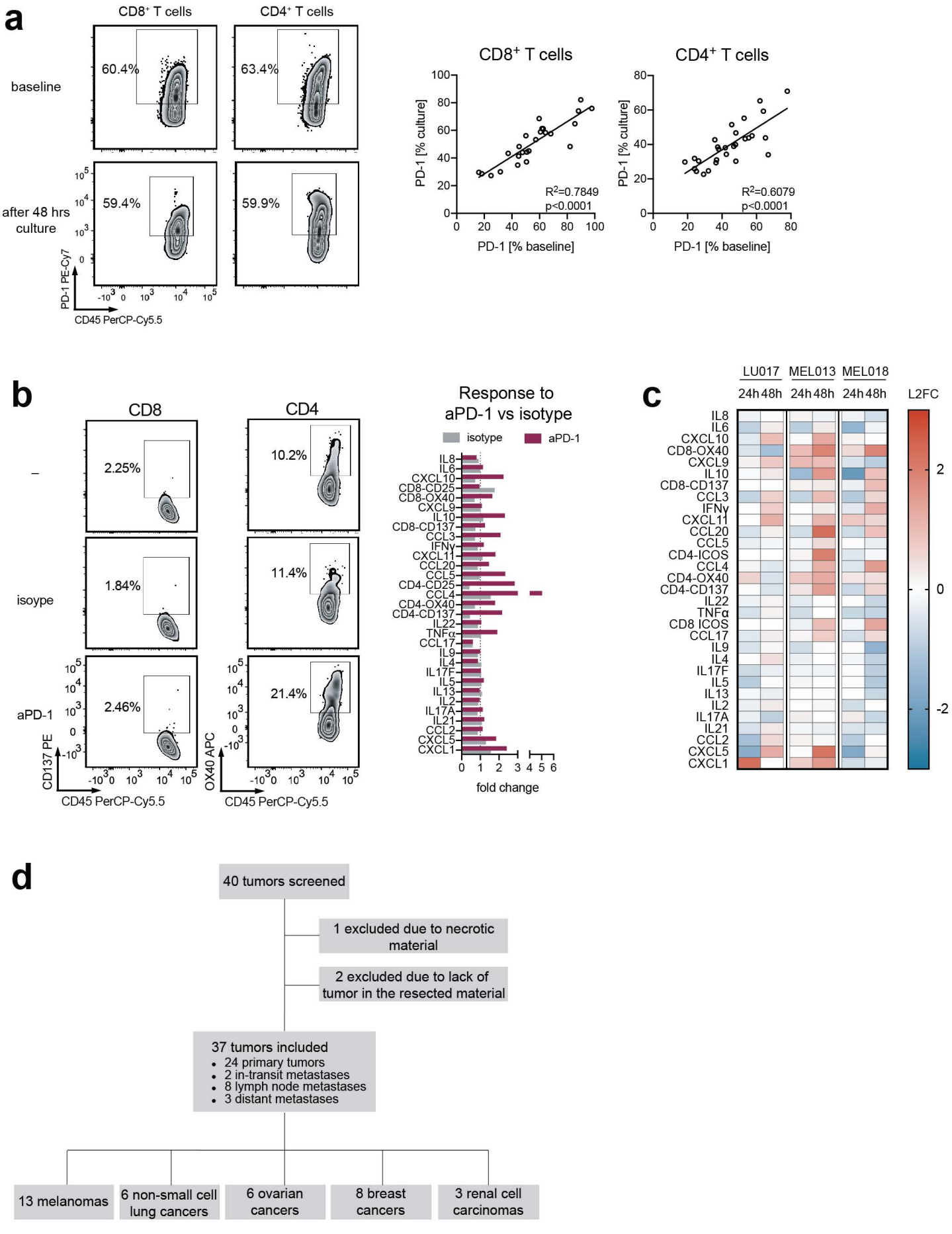

Extended Data Figure 3

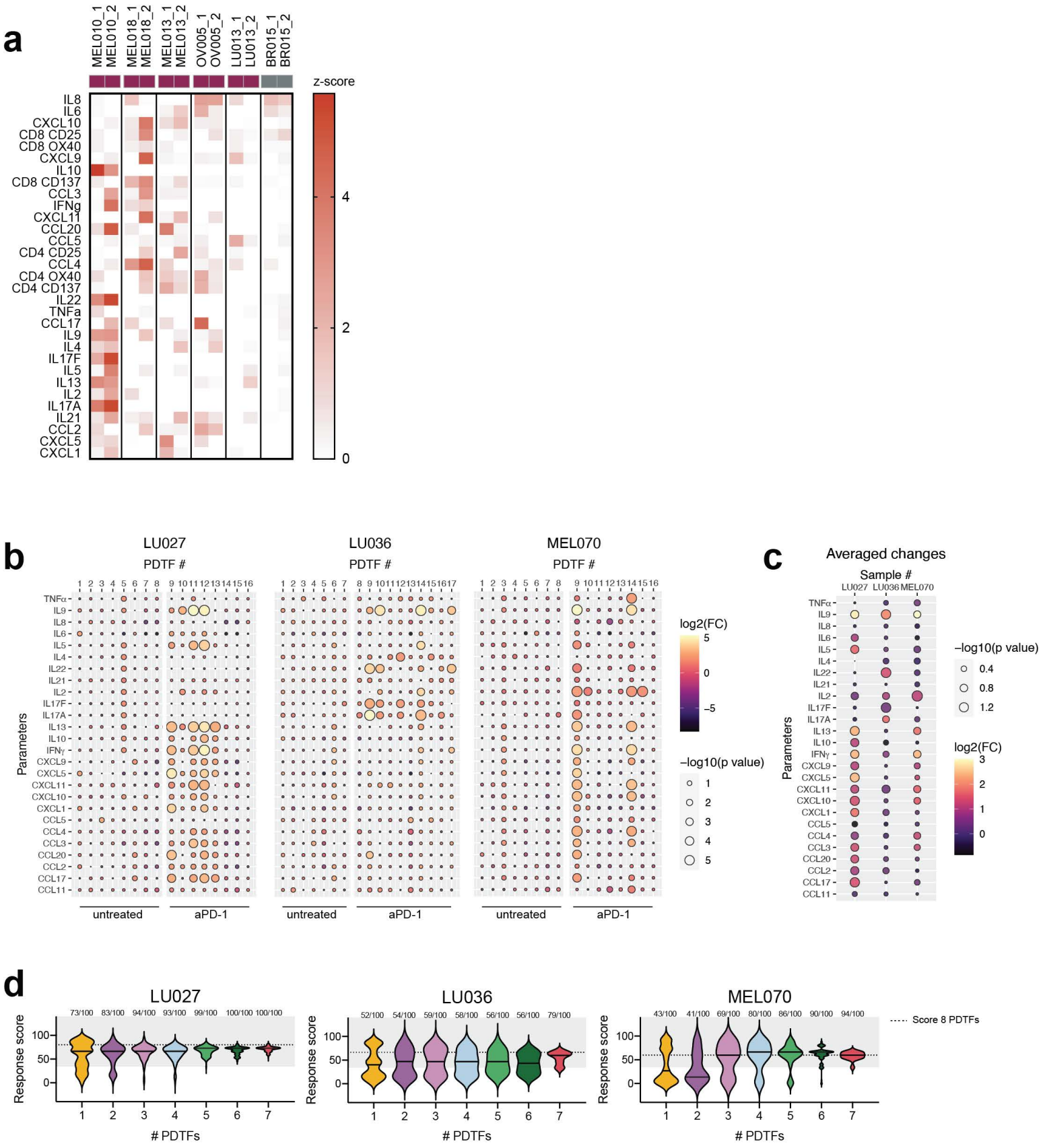

Extended Data Figure 4

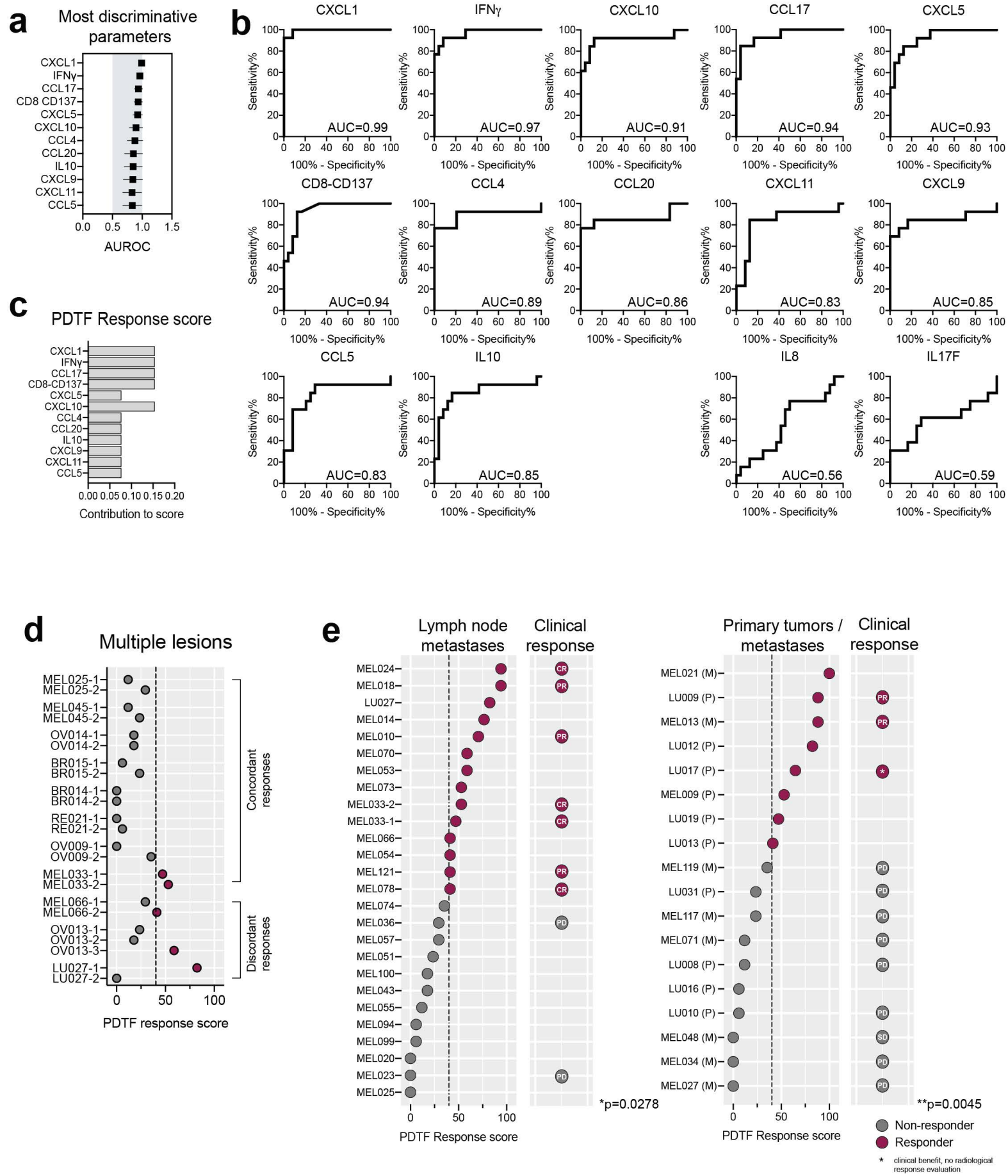

Extended Data Figure 5

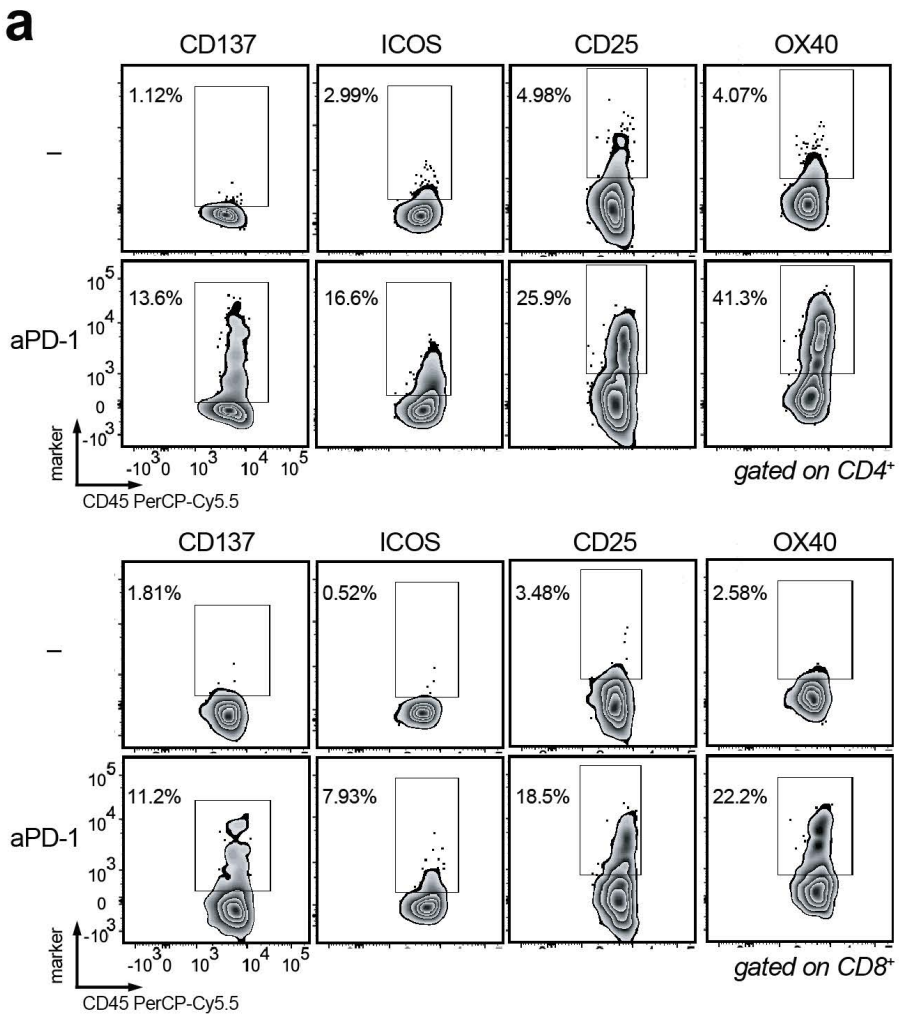

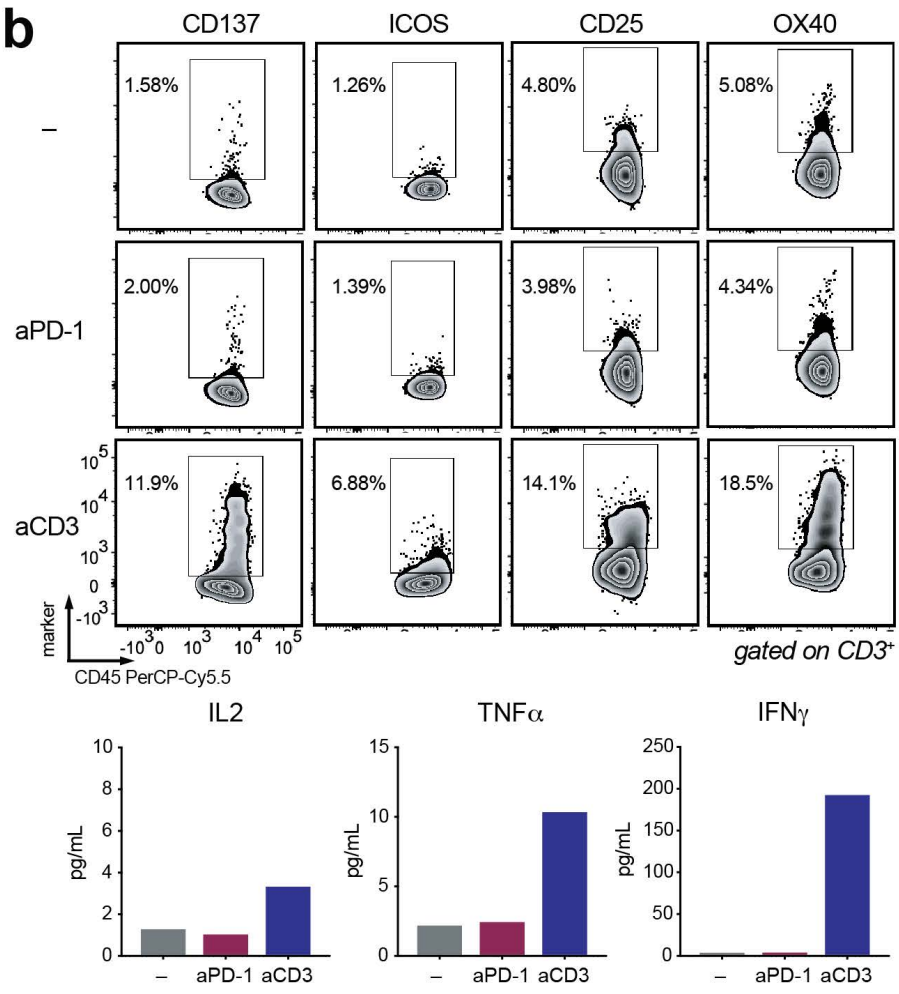

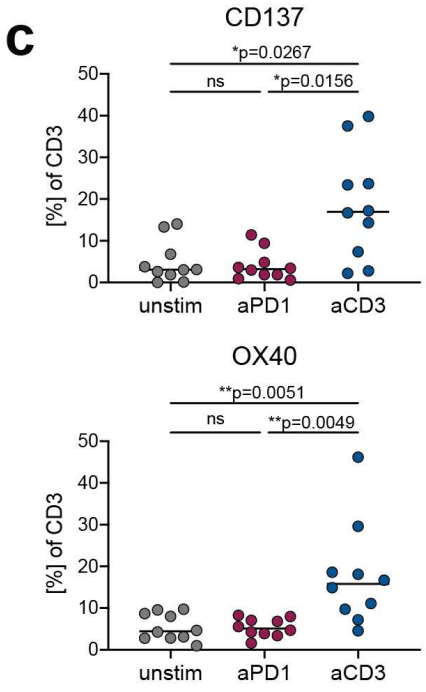

Extended Data Figure 6

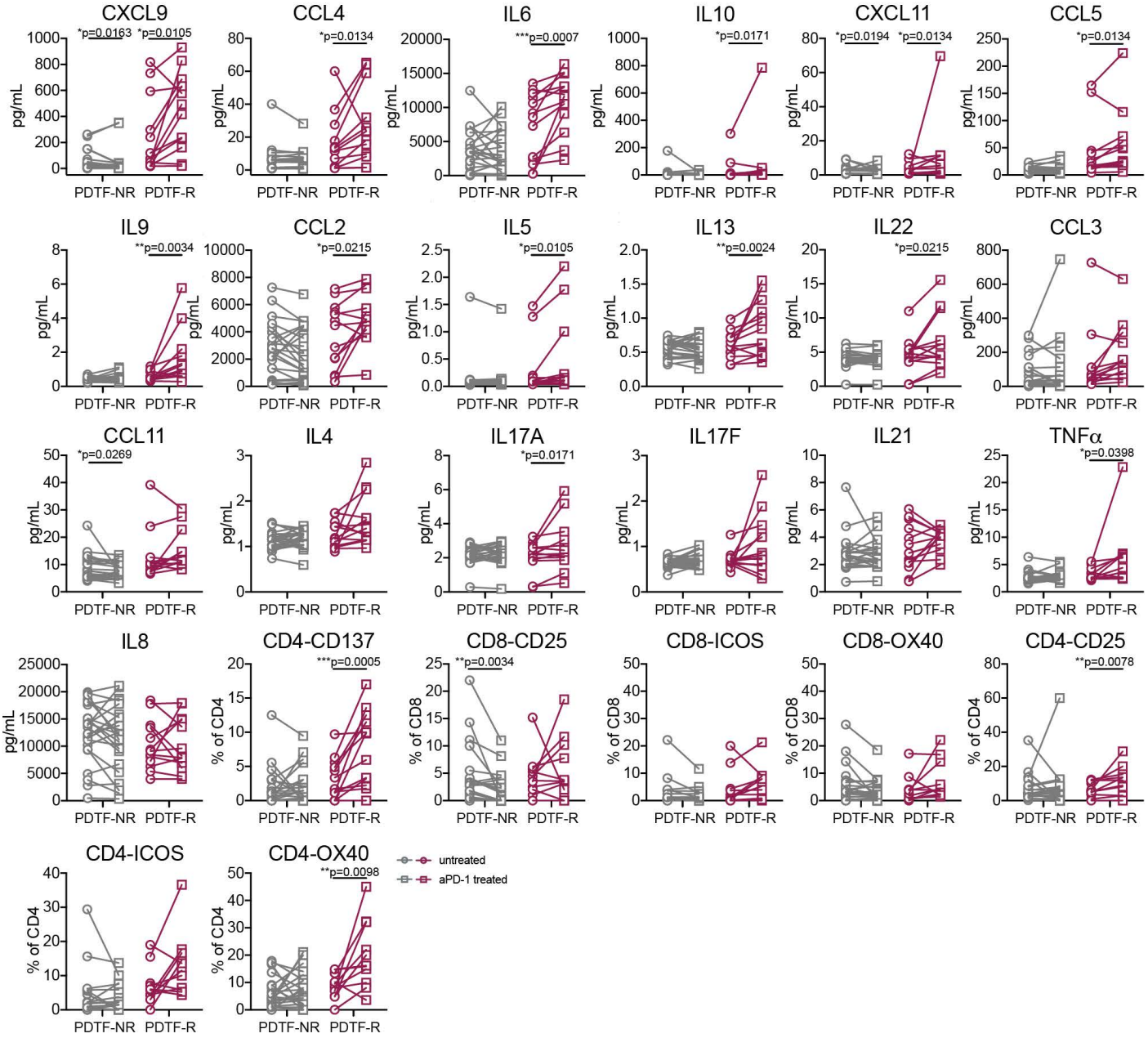

Extended Data Figure 7

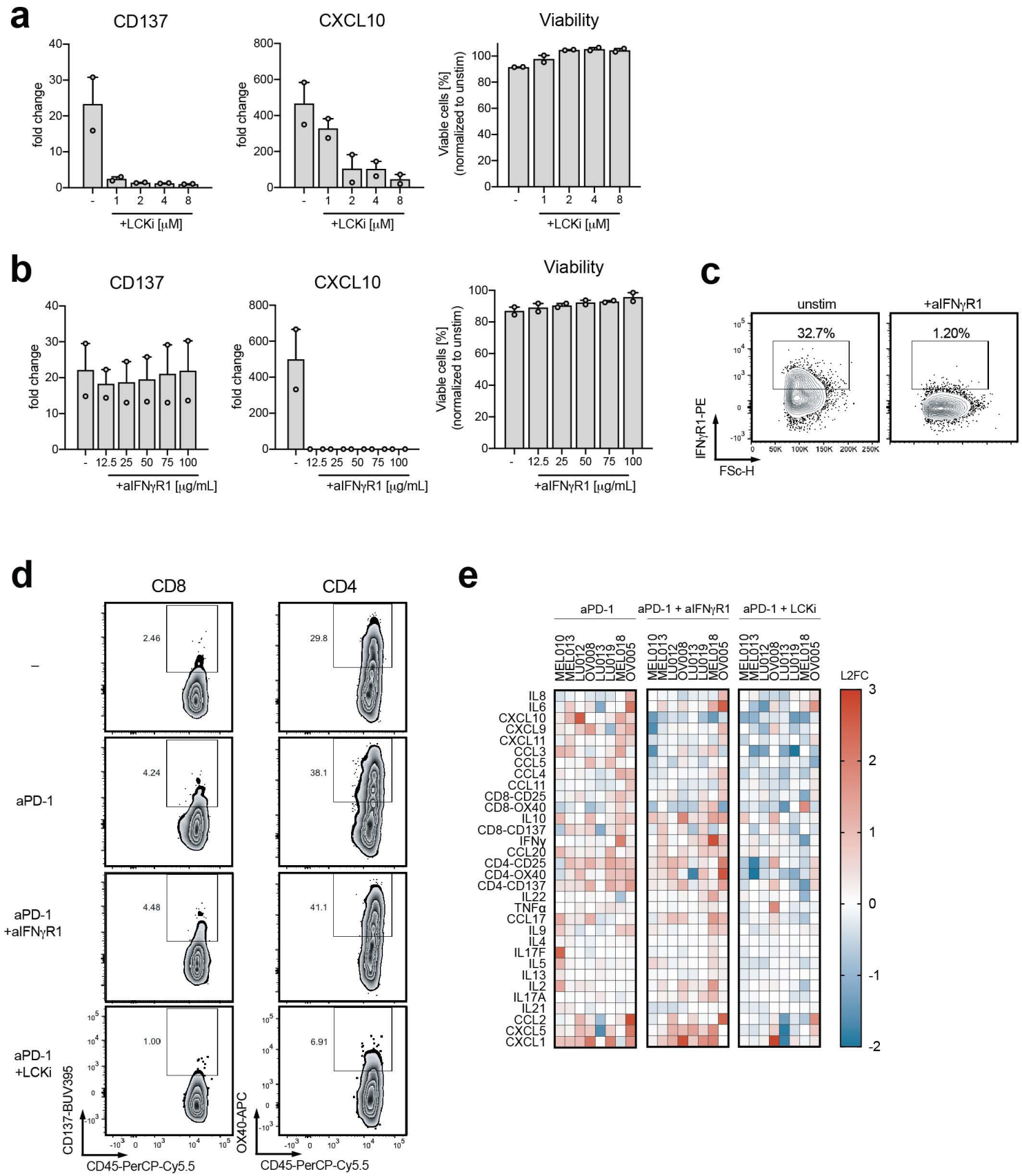

Extended Data Figure 8

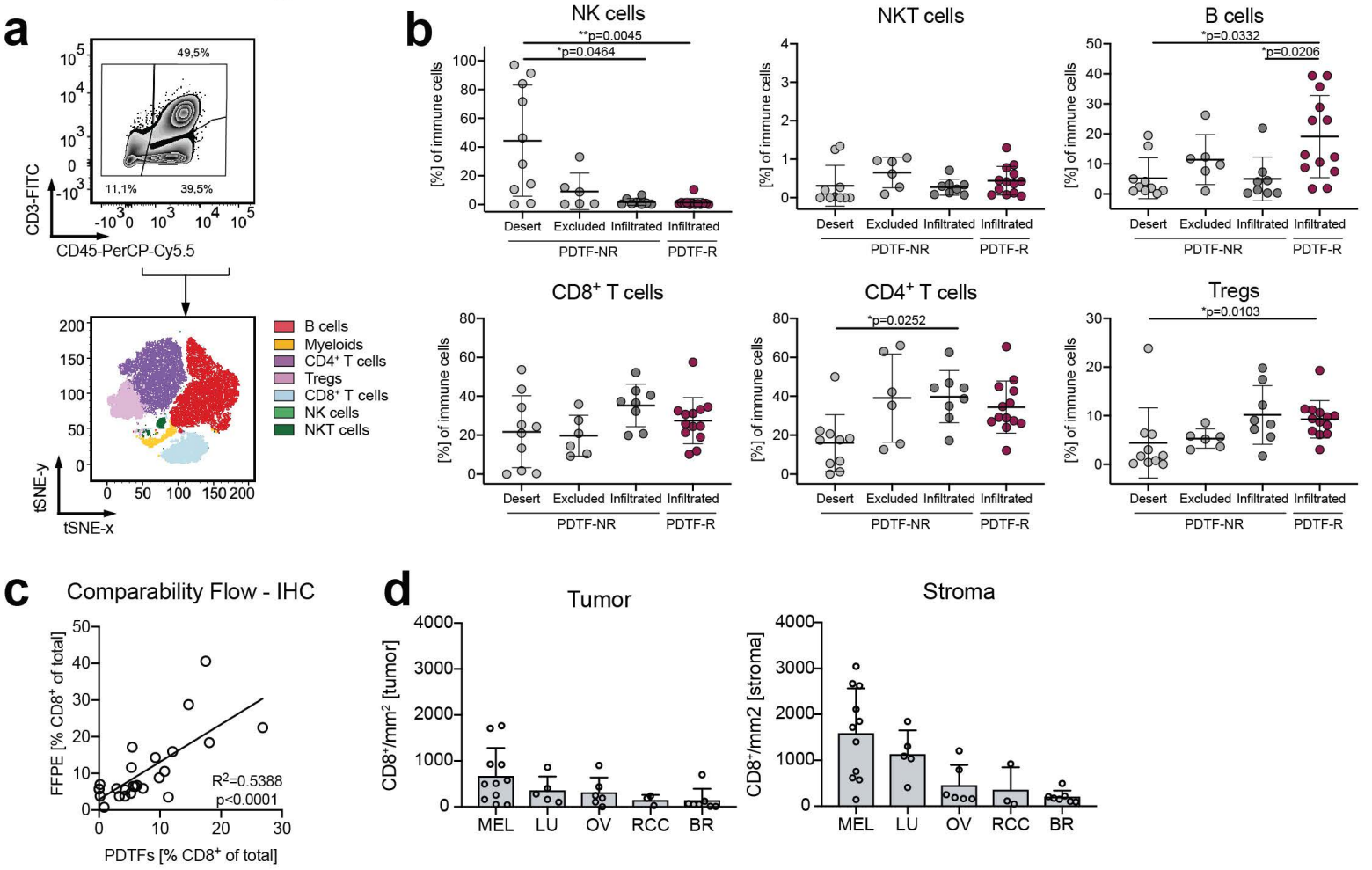

Extended Data Figure 9

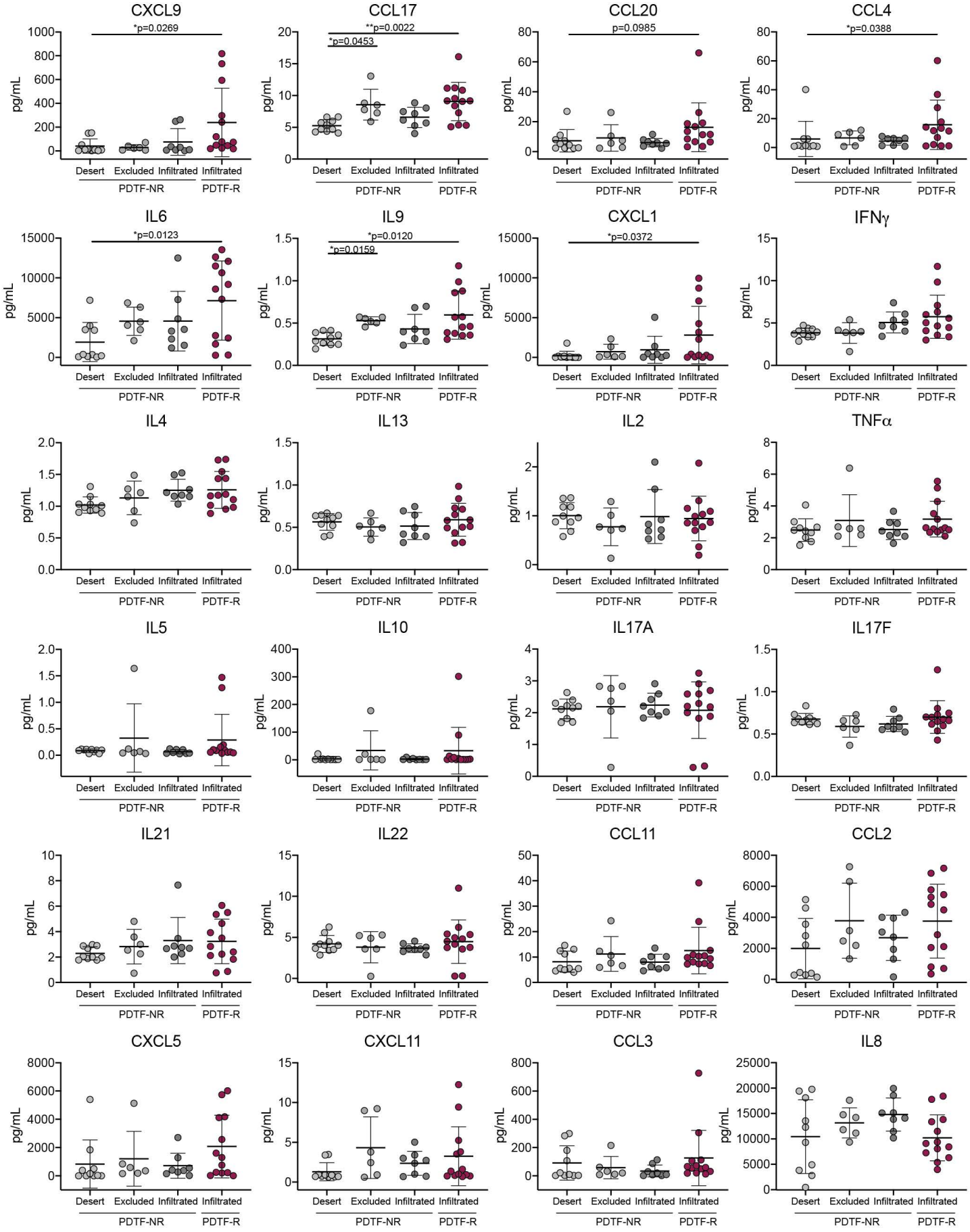

Extended Data Figure 10

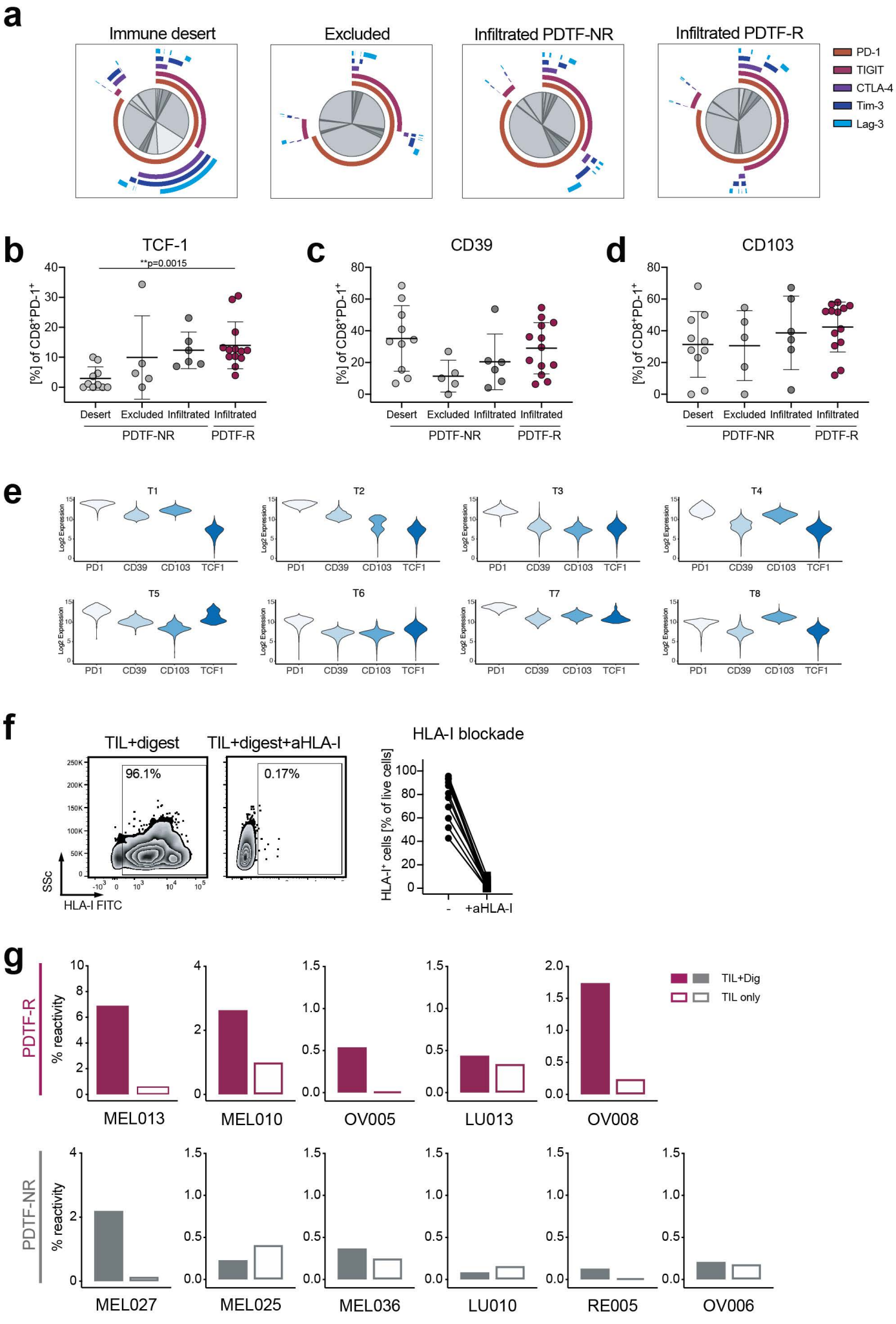

Supplementary Figures

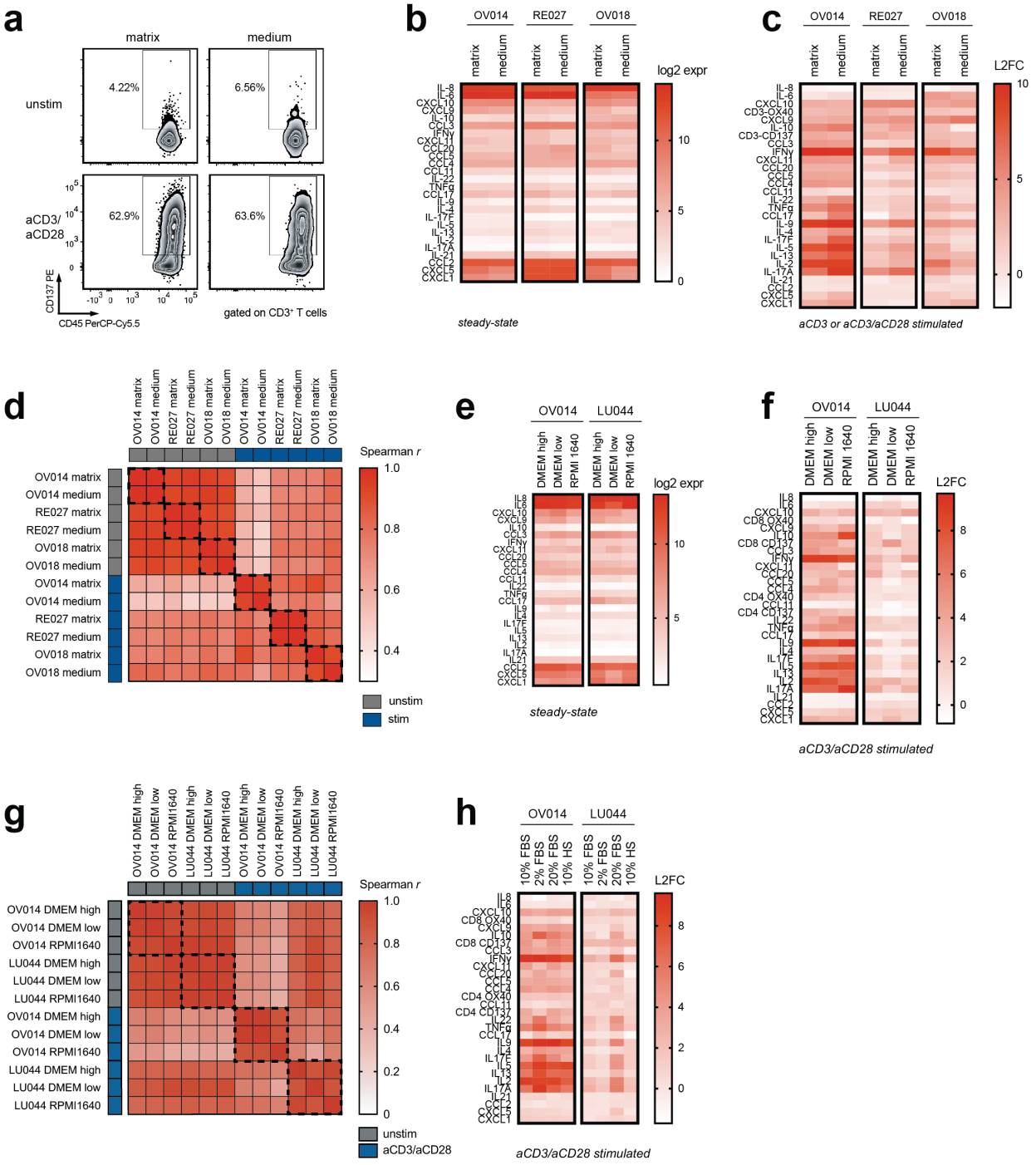

Supplementary Figure 1. PDTF culture maintenance. a-c, Flow plots showing CD137 expression on CD3+ T cells (**a**) and heatmaps indicating cytokine and chemokine secretion and T cell activation in untreated (**b**, log2-transformed data) and stimulated (**c**, log2 fold change to untreated) PDTFs that were either cultured in matrix or in medium alone. OV014 was stimulated with aCD3/aCD28, RE027 and OV018 were stimulated with aCD3 only. **d**, Correlation matrix depicting the Spearman co-efficient of cytokine/chemokine measurements and activation markers at 48 hrs in unstimulated and stimulated PDTFs that were either cultured in matrix or in medium. **e-h**, Heatmaps showing cytokine/chemokine secretion and T cell activation in untreated (**e**, log2-transformed data) and aCD3/aCD28 stimulated (**f**, log2 fold change to untreated) PDTFs that were cultured in different glucose concentrations (DMEM high 4,500 mg/L, DMEM low 1,000 mg/L, RPMI1640 2,000 mg/L). **g**, Correlation matrix depicting the Spearman co-efficient of cytokine/chemokine measurements and activation markers at 48 hrs in unstimulated and stimulated PDTFs that were cultured in different glucose concentrations. **h**, Heatmap showing cytokine/chemokine secretion and T cell activation in aCD3/aCD28 stimulated (log2 fold change to untreated) PDTFs that were cultured in different fetal bovine serum (FBS) or human serum (HS) concentrations.

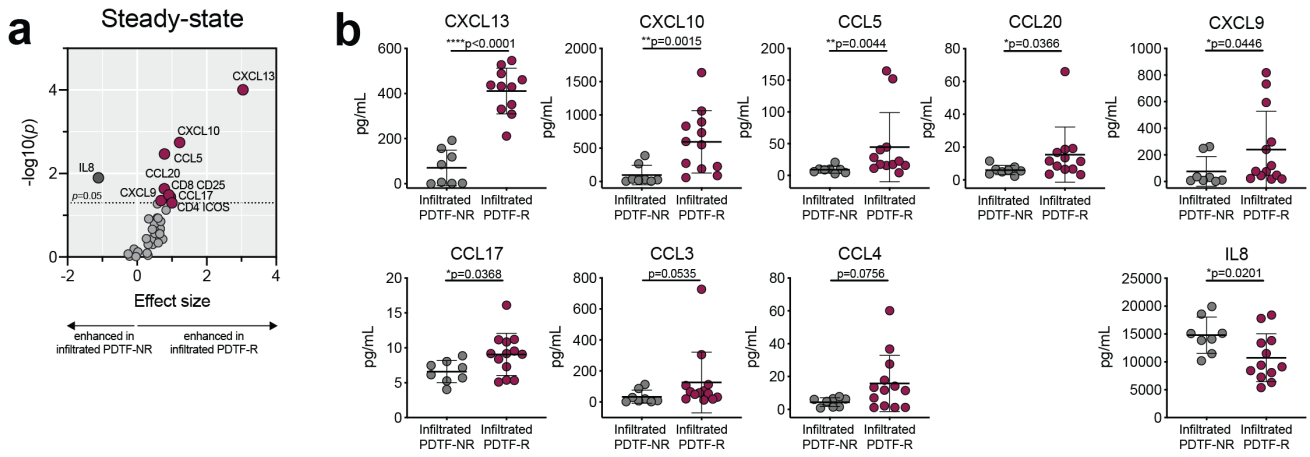

Supplementary Figure 2. Comparison of infiltrated PDTF-NR and PDTF-R tumors. a, Effect size (calculated by Hedge's g) and *p* values (by two-tailed Mann-Whitney test) of differences in steady-state cytokine and chemokine production between infiltrated PDTF-R and PDTF-NR. **b**, Most differentially expressed cytokines and chemokines between infiltrated PDTF-R and PDTF-NR (n=21 tumors). Shown are mean +/- s.d., *p<0.05, **p<0.01, ****p<0.0001 by two-tailed Mann-Whitney test.

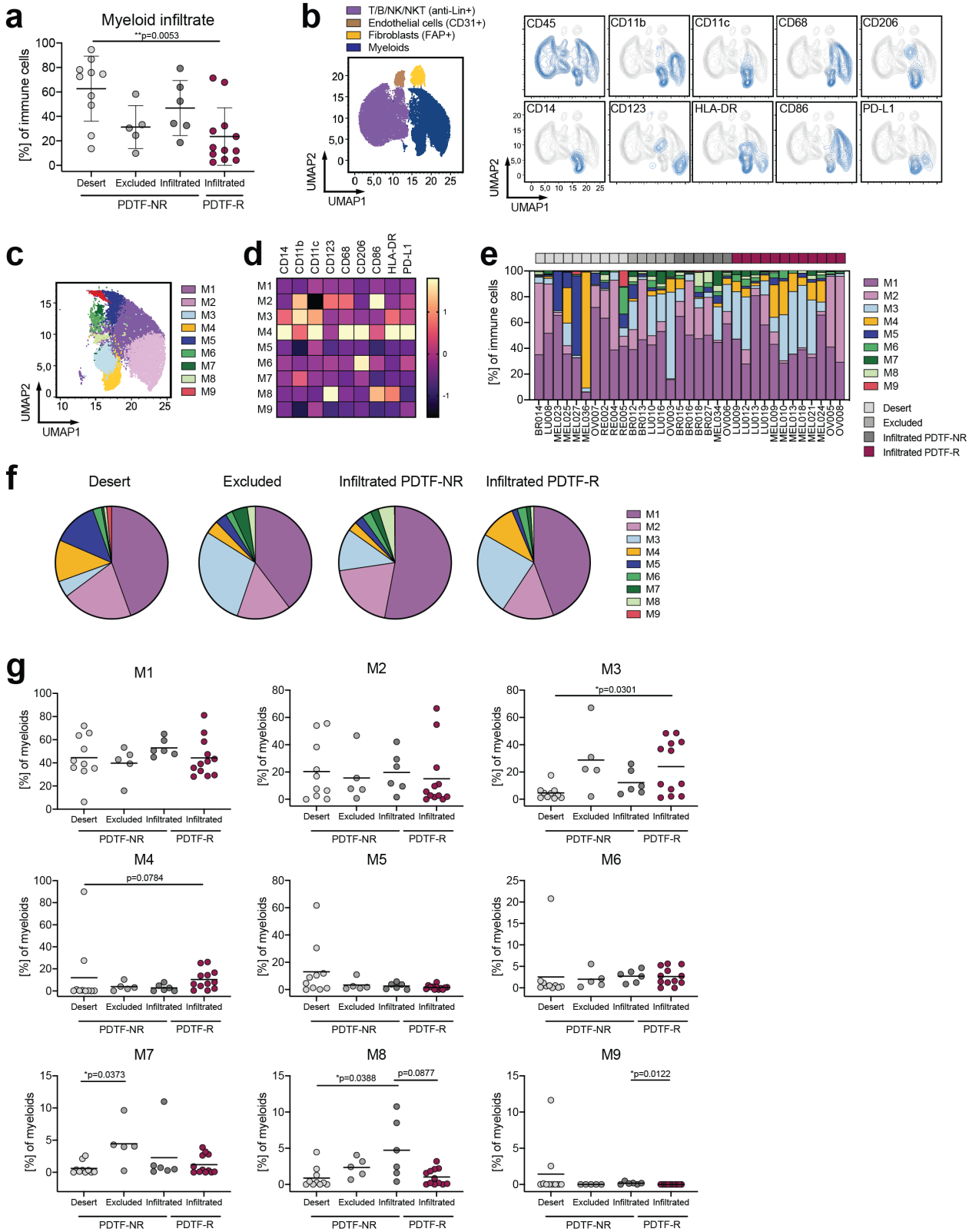
a
Myeloid infiltrate
**p=0.0053
[%] of immune cells
Desert
Excluded
Infiltrated
Infiltrated
PDTF-NR
PDTF-R
b
T/B/NK/NKT (anti-Lin+)
Endothelial cells (CD31+)
Fibroblasts (FAP+)
Myeloids
UMAP2
UMAP1
CD45
CD11b
CD11c
CD68
CD206
CD14
CD123
HLA-DR
CD86
PD-L1
c
M1
M2
M3
M4
M5
M6
M7
M8
M9
d
e
[%] of immune cells
Desert
Excluded
Infiltrated PDTF-NR
Infiltrated PDTF-R
f
Desert
Excluded
Infiltrated PDTF-NR
Infiltrated PDTF-R
g
M1
M2
M3
*p=0.0301
M4
p=0.0784
M5
M6
M7
*p=0.0373
M8
*p=0.0388
p=0.0877
M9
*p=0.0122
[%] of myeloids

Supplementary Figure 3. Analysis of infiltrating myeloid subsets. a, Quantification of the myeloid infiltrate within total immune cells ($CD45^+$) for the four distinct TME subtypes (n=32). Shown are mean +/- s.d., $^{**}p<0.01$ by Kruskal-Wallis test corrected for multiple comparisons. **b**, UMAP clustering of lymphoid, myeloid, fibroblast and endothelial cell subsets (left). Overlay plots indicating expression of the markers used for assessment of myeloid cells. **c**, Depiction of myeloid clusters on the UMAP plot. **d**, Normalized expression of different myeloid markers on the nine identified myeloid clusters. **e**, Quantification of the myeloid clusters within total immune cells ($CD45^+$) in each tumor. **f**, Pie charts indicating the distribution of myeloid clusters per TME subgroup. **g**, Quantification of myeloid clusters in all TME groups. $^{*}p<0.05$ by Kruskal-Wallis test corrected for multiple comparisons.

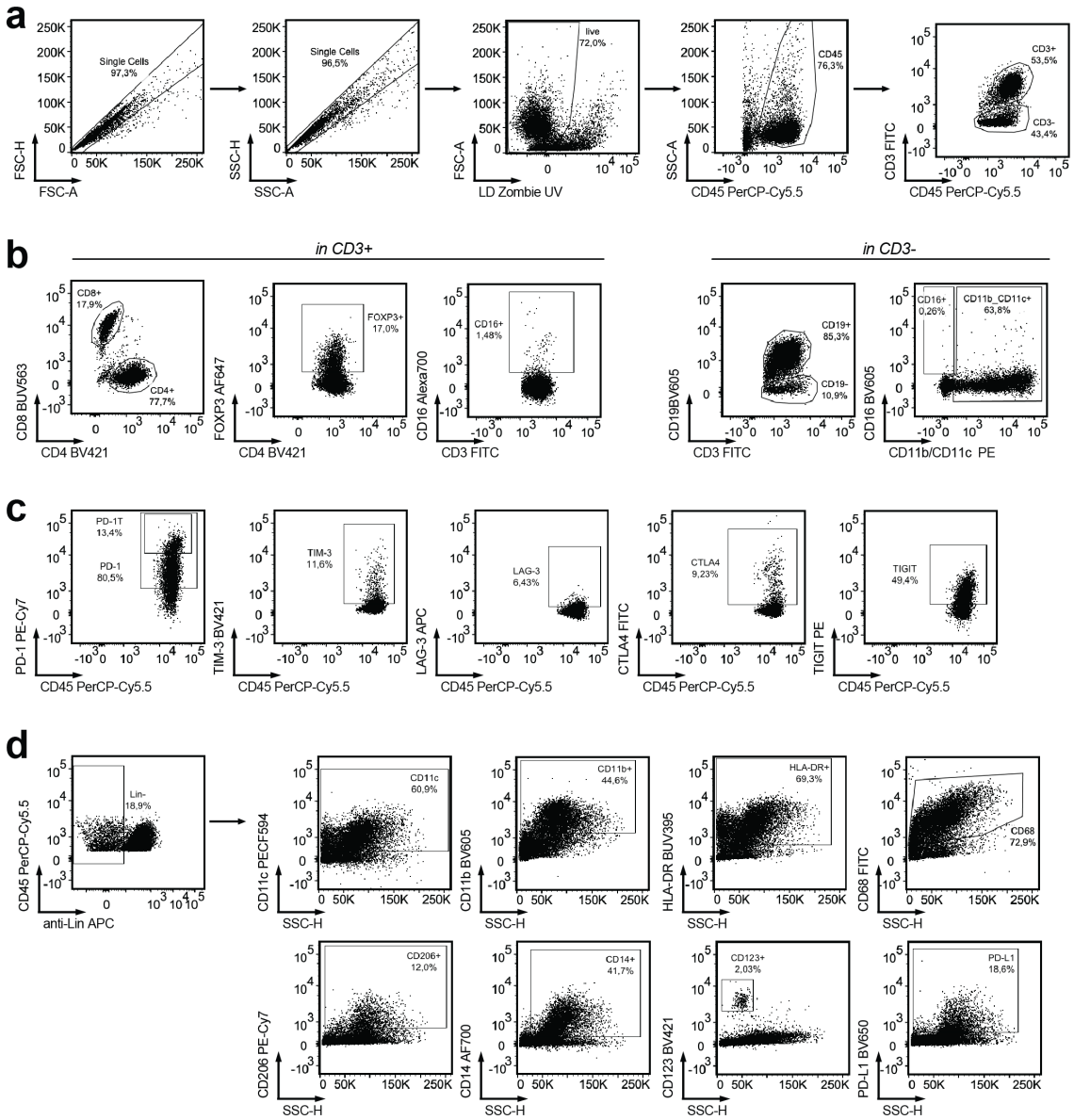

Supplementary Figure 4. Gating strategy and marker expression. a, Gating strategy used for all flow cytometry experiments and for sorting. **b**, Flow plots showing the expression of all markers used to identify major immune cell subsets either within CD3+ or CD3- subsets. **c**, Flow plots showing the expression of inhibitory receptors gated on CD8+ T cells. **d**, Flow plots showing the expression of myeloid markers gated within the Lin- population.

Supplementary Table 1. Patient characteristics

Patient ID	Histology	Tumor site	Systemic treatment with anti-PD-1	Clinical response	Ex vivo response to anti-PD-1
Breast cancer					
BR012	Ductal carcinoma	Primary	no	NA	PDTF-NR
BR013	Ductal carcinoma	Primary	no	NA	PDTF-NR
BR014	Ductal carcinoma	Primary	no	NA	PDTF-NR
BR015	Lobular carcinoma	Primary	no	NA	PDTF-NR
BR016	Ductal carcinoma	Primary	no	NA	PDTF-NR
BR017	Ductal carcinoma	Primary	no	NA	PDTF-NR
BR018	Lobular carcinoma	Primary	no	NA	PDTF-NR
BR027	Lobular carcinoma mixed with other carcinoma type	Primary	no	NA	PDTF-NR
Non-small cell lung cancer					
LU008	Adenocarcinoma	Primary	yes	Progressive disease	PDTF-NR
LU009	Adenocarcinoma	Primary	yes	Partial response	PDTF-R
LU010	Acinary adenocarcinoma	Primary	no	NA	PDTF-NR
LU012	Acinary adenocarcinoma	Primary	no	NA	PDTF-R
LU013	Adenocarcinoma with neuroendocrine differentiation	Primary	no	NA	PDTF-R
LU016	Acinar cell cystadenocarcinoma	Primary	no	NA	PDTF-NR
LU019	Non-small-cell carcinoma	Primary	no	NA	PDTF-R
Melanoma					
MEL009	Lentigo maligna melanoma	Primary	no	NA	PDTF-R
MEL010	Malignant melanoma, not specified	Lymph node metastasis	yes	Partial response	PDTF-R
MEL013	Nodular melanoma	Subcutaneous metastasis	yes	Partial response	PDTF-R
MEL014	Superficial spreading melanoma	Lymph node metastasis	no	NA	PDTF-R
MEL018	Nodular melanoma	Lymph node metastasis	yes	Partial response	PDTF-R
MEL020	Superficial spreading melanoma	Lymph node metastasis	no	NA	PDTF-NR
MEL021	Superficial spreading melanoma	Lung metastasis	no	NA	PDTF-R
MEL023	Malignant melanoma	Lymph node metastasis	yes	Progressive disease	PDTF-NR
MEL024	Superficial spreading melanoma	Lymph node metastasis	yes	Complete response	PDTF-R
MEL025	Malignant melanoma, not specified	Lymph node metastasis	no	NA	PDTF-NR
MEL027	Acrolentiginous melanoma	Lung metastasis	yes	Progressive disease	PDTF-NR
MEL034	Superficial spreading melanoma	Subcutaneous metastasis	yes	Progressive disease	PDTF-NR
MEL036	Malignant melanoma, not specified	Lymph node metastasis	yes	Progressive disease	PDTF-NR
Ovarian cancer					
OV001	Clear cell adenocarcinoma	Primary	no	NA	PDTF-NR
OV003	Adenocarcinoma	Primary	no	NA	PDTF-NR
OV005	Serous cystadenocarcinoma	Primary	no	NA	PDTF-R

OV006	Serous cystadenocarcinoma	Peritoneal metastasis	no	NA	PDTF-NR
OV007	Mucinous adenocarcinoma	Primary	no	NA	PDTF-NR
OV008	Serous cystadenocarcinoma	Primary	no	NA	PDTF-R
Renal cell carcinoma					
RE002	Clear cell adenocarcinoma	Primary	no	NA	PDTF-NR
RE004	Clear cell adenocarcinoma	Primary	yes	Progressive disease	PDTF-NR
RE005	Chromophobic carcinoma	Primary	no	NA	PDTF-NR

Supplementary Table 2. Patient characteristics – Validation cohort

Patient ID	Histology	Tumor site	Systemic treatment with anti-PD-1	Clinical response	Ex vivo response to anti-PD-1
Breast cancer					
BR007	Ductal carcinoma	Primary	yes	Progressive disease	PDTF-NR
Non-small cell lung cancer					
LU017	Acinar cell / cystadenocarcinoma	Primary	yes	Clinical benefit*	PDTF-R
LU031	Large cell carcinoma	Primary	yes	Progressive disease	PDTF-NR
LU032	Adenocarcinoma	Metastasis (adrenal gland)	yes#	Progressive disease#	PDTF-NR
LU033	Squamous cell carcinoma	Primary	yes#	Progressive disease#	PDTF-NR
Melanoma					
MEL033-1	Nodular melanoma	Lymph node metastasis	yes	Complete response	PDTF-R
MEL033-2	Nodular melanoma	Lymph node metastasis	yes	Complete response	PDTF-R
MEL044	Superficial spreading melanoma	Subcutaneous metastasis	yes#	Progressive disease#	PDTF-NR
MEL046	Superficial spreading melanoma	Metastasis (lung)	yes#	Progressive disease#	PDTF-NR
MEL047	Malignant melanoma (not specified)	Metastasis (adrenal gland)	yes#	Progressive disease#	PDTF-NR
MEL048	Nodular melanoma	Metastasis (lung)	yes	Stable disease	PDTF-NR
MEL069	Nodular melanoma	Lymph node metastasis	yes	Mixed response	PDTF-R
MEL071	Superficial spreading melanoma	Subcutaneous metastasis	yes	Progressive disease	PDTF-NR
MEL074	Spindle cell melanoma	Lymph node metastasis	yes	Mixed response	PDTF-NR
MEL075	Superficial spreading melanoma	Subcutaneous metastasis	yes#	Progressive disease#	PDTF-NR
MEL078	Superficial spreading melanoma	Lymph node metastasis	yes	Complete response	PDTF-R
MEL081	Nodular melanoma	Lymph node metastasis	yes	Mixed response	PDTF-R
MEL084	Superficial spreading melanoma	Metastasis (adrenal gland)	yes#	Progressive disease#	PDTF-NR
MEL094	Superficial spreading melanoma	Lymph node metastasis	yes#	Progressive disease#	PDTF-NR
MEL097	Superficial spreading melanoma	Subcutaneous metastasis	yes#	Progressive disease#	PDTF-NR
MEL115	Malignant melanoma, not specified	Lymph node metastasis	yes#	Progressive disease#	PDTF-NR
MEL117	Malignant melanoma, not specified	In transit metastasis	yes	Progressive disease	PDTF-NR
MEL118	Superficial spreading melanoma	Metastasis (adrenal gland)	yes#	Progressive disease#	PDTF-NR
MEL119	Malignant melanoma, not specified	Subcutaneous metastasis	yes	Progressive disease	PDTF-NR
MEL120	Superficial spreading melanoma	Lymph node metastasis	yes#	Progressive disease#	PDTF-NR
MEL121	Malignant melanoma, not specified	Lymph node metastasis	yes	Partial responder	PDTF-R

*No radiological response evaluation, death to non-cancer related cause

#aPD-1 resistant lesion

Supplementary Table 3. Patient characteristics – Multiple lesions cohort

Patient ID	Lesion	Histology	Tumor site	Ex vivo response to anti-PD-1
MEL025	1	Malignant melanoma, not specified	Lymph node metastasis	PDTF-NR
	2	Malignant melanoma, not specified	Lymph node metastasis	PDTF-NR
MEL033	1	Nodular melanoma	Lymph node metastasis	PDTF-R
	2	Nodular melanoma	Lymph node metastasis	PDTF-R
MEL045	1	Superficial spreading melanoma	Subcutaneous metastasis	PDTF-NR
	2	Superficial spreading melanoma	Subcutaneous metastasis	PDTF-NR
MEL066	1	Malignant melanoma, not specified	Lymph node metastasis	PDTF-NR
	2	Malignant melanoma, not specified	Subcutaneous metastasis	PDTF-R
LU027	1	Adenocarcinoma lung	Lymph node metastasis	PDTF-R
	2	Adenocarcinoma lung	Primary	PDTF-NR
BR014	1	Ductal carcinoma breast	Primary (left breast)	PDTF-NR
	2	Ductal carcinoma breast	Primary (right breast	PDTF-NR
BR015	1	Lobular carcinoma breast	Primary	PDTF-NR
	2	Lobular carcinoma breast	Lymph node metastasis	PDTF-NR
RE021	1	Chromophobic renal carcinoma	Multinodular primary tumor (hemorrhagic part)	PDTF-NR
	2	Chromophobic renal carcinoma	Multinodular primary tumor (fatty part)	PDTF-NR
OV009	1	Serous cystadenocarcinoma ovary	Primary	PDTF-NR
	2	Serous cystadenocarcinoma ovary	Metastasis (omentum)	PDTF-NR
OV013	1	Endometrioid adenocarcinoma ovary	Primary	PDTF-NR
	2	Endometrioid adenocarcinoma ovary	Metastasis (omentum)	PDTF-NR
	3	Endometrioid adenocarcinoma ovary	Metastasis (peritoneum)	PDTF-R
OV014	1	Serous adenocarcinoma ovary	Metastasis (omentum)	PDTF-NR
	2	Serous adenocarcinoma ovary	Primary	PDTF-NR